
DEUP: Direct Epistemic Uncertainty Estimation

Salem Lahlou*

Mila, Université de Montréal

Moksh Jain*

Mila, Université de Montréal

Hadi Nekoei

Mila, Université de Montréal

Victor I Butoi

Cornell University

Paul Bertin

Mila, Université de Montréal

Jarrid Rector-Brooks

Mila, Université de Montréal

Maksym Korablyov

Mila, Université de Montréal

Yoshua Bengio

Mila, Université de Montréal, CIFAR Fellow

Abstract

Epistemic Uncertainty (EU) is the part of out-of-sample prediction error due to the lack of knowledge of the learner. While existing work focuses on model variance as a proxy of EU, we propose a principled framework for directly estimating it by learning to predict the generalization error and subtracting an estimate of aleatoric uncertainty, i.e., intrinsic unpredictability, using a secondary learner. We discuss the merits of this novel interpretation of EU, and highlight how it differs from variance-based proxies of EU and addresses their shortcomings. Our framework, Direct Epistemic Uncertainty Prediction (DEUP) is particularly interesting in interactive learning environments, where the learner is allowed to acquire novel examples in each round. Through a wide set of experiments, we illustrate how existing methods in sequential model optimization can be improved with EU estimates from DEUP, and how DEUP can be used to drive exploration in reinforcement learning. We also evaluate the quality of uncertainty estimates from DEUP for probabilistic image classification and predicting synergies of drug combinations.

A remaining great challenge for machine learning research is purposeful knowledge-seeking by learning agents, which can benefit from estimation of epistemic uncertainty, i.e., a measure of lack of knowledge. The epistemic uncertainty can potentially be eliminated with enough data if the learner converges to a Bayes-optimal predictor, i.e. one with the lowest possible expected loss at every input point. EU estimation is already a key ingredient in active learning and Sequential Model Optimization (SMO) [2, 21] as well as exploration in Reinforcement Learning (RL) [36, 71]. EU estimators can tell us how much could be gained from learning around a particular area of state-space or input data space. But how should we even quantify it? Much previous work has focused on model variance [22, 40] as a proxy thereof, i.e., how different from each other are functions compatible with the data and with the learner’s preferences (for instance the choice of the parametric family or learning algorithms). In interactive learning settings like active learning or RL, the model variance estimated only using the currently available data is used as a proxy of EU for acquiring new data. This, as we posit below, has two fundamental limitations:

- At each step of interactive learning, the learner observes a gap between the observed values at the acquired points and its prediction at those points. Yet, this gap is typically not used to calibrate its uncertainty estimates at similar points in the next acquisition steps. As an illustration for this issue, consider the function shown in Fig. 1 (top, in black), and an interactive learner that seeks to improve its estimate of the ground-truth function by acquiring more points. If the acquisition relies on a variance-based proxy of EU (as in Fig. 1 with a Gaussian Process, or GP), then the

*Equal Contribution, Correspondence to: lahlosal@mila.quebec, mokshjn00@gmail.com

EU estimate might even become worse in regions where the learner (post acquisition) knows it underestimated the uncertainty. In other words, there is no reason for such a learner to extrapolate the mismatch between the predicted error and the true error (which we show below to be related to EU) to similar points in subsequent rounds. In this example, where we consider one round of acquisition, there is no mechanism that allows the second GP to look at the first GP’s variance and the ground-truth value of the acquired points in order to adjust its own variance estimates in that region, which should ideally be larger considering the poor calibration in the round before.

- In most cases, the learner has some bias (misspecification) associated with it, due to finite capacity or preferences, self-imposed to avoid overfitting. Particularly in the case of neural network learners, the capacity can be increased with more data and more training: for example, early stopping will choose a higher effective capacity with more data. This bias, which is not incorporated in the model variance, is important to account for in the EU. Recent work [50, 13] has also shown that parametric Bayesian methods are suboptimal for learning predictive models when the model is misspecified. In Section 1, we expand on the brittle relationship between model variance and EU, which can get murky in the presence of bias or the very coarse approximations of the posterior distribution over neural networks that are typically used, e.g., with MC-Dropout [22] or Deep Ensembles [40].

Motivated by interactive learning settings arising for example in SMO and RL, we study —as an alternative or complement—the quantification of EU in terms of out-of-sample loss, which does include the bias term discussed above, and allows for recalibration as more data is acquired. However, the total expected out-of-sample loss at a point includes not just EU (reducible loss) but also an aleatoric (irreducible) part. *We thus propose a definition of EU as the difference between the expected generalization error and aleatoric uncertainty.* Estimating it is useful to an interactive learner because it could be reduced with enough data, especially in regions of the input space we care about, i.e., where EU is large. We thus propose DEUP, for Direct Epistemic Uncertainty Prediction, where we train a side learner (the uncertainty predictor) with an appropriate objective and appropriate data in order to predict this generalization error, and then subtract an estimate of aleatoric uncertainty which can be estimated using multiple samples from the oracle as discussed in Sec. 2. Note that our method is agnostic to the particular search method still needed to select points with high EU in order to propose new candidates for active learning [2, 57, 7] or SMO [39, 30, 67], or exploration in RL [36, 59, 29].

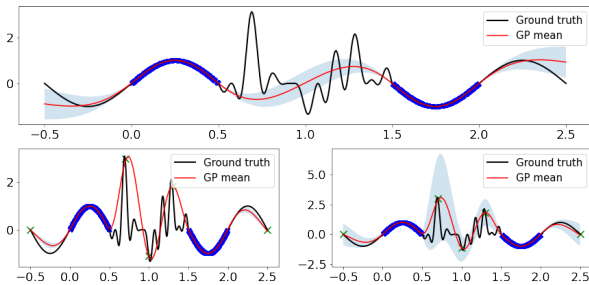


Figure 1: *Top.* A GP is fit on (dark blue) points in $[0, 0.5] \cup [1.5, 2]$. The shaded area represents the GP standard deviation, often used as a proxy for epistemic uncertainty. *Bottom left.* A second GP fit on the same points, with 5 extra points (green). This second GP predicts almost 0 standard deviation everywhere, even though the first GP significantly underestimated the uncertainty in $[0.5, 1.5]$, because no signal is given to the learner that the region $[0.5, 1.5]$ should be explored more. *Bottom right.* DEUP learns to map the underestimated variances of the first GP to the L2 errors made by that GP, and yields more reasonable uncertainty estimates that should inform the learner of what area to explore.

A unique advantage of DEUP, compared with methods relying on model variance, is that it can be explicitly trained to care about, and calibrate for estimating the uncertainty for examples which may come from a distribution slightly different from the distribution of most of the training examples. Such distribution shifts arise naturally in contexts like active learning and RL because the learner explores new areas of the input space. In these non-stationary settings, we typically want to retrain the main predictor as we acquire new training data, not just because more training data is generally better but also to better track the changing distribution and generalize to yet unseen but upcoming OOD inputs. This setting makes it challenging to train the main predictor but it also entails a non-stationarity for the training data seen by the error predictor: a large error initially made at a point x before x is incorporated in the training set (along with an outcome y) will typically be greatly reduced after updating the main predictor with (x, y) .

To cope with this non-stationarity in the targets of the error predictor, we propose in Sec. 2.2 to use additional features as input to the uncertainty estimator, that are informative of both

the input point and the dataset used to obtain the current predictor. We mainly use density estimates and model variance estimates, that sometimes come at no additional cost.

In summary, the main contributions of this paper are the following:

- In Sec. 1, we propose a definition of epistemic uncertainty as the reducible part of generalization error, and discuss how this novel interpretation addresses the shortcomings of variance-based proxies of EU.
- In Sec. 2, we present DEUP, a principled framework for estimating epistemic uncertainty that is particularly interesting in interactive settings, and propose a means to mitigate the issue of non-stationarity arising in such settings.
- In Sec. 4, we experimentally show how EU estimates from DEUP can improve upon existing SMO methods and drive exploration in RL. We then evaluate the quality of these uncertainty estimates in probabilistic image classification and in a regression task predicting synergies of drug combinations.

1 Aleatoric and Epistemic Uncertainty

Consider a supervised learning algorithm (or learner) \mathcal{L} mapping a dataset \mathcal{D} to a predictive function $\hat{f} = \mathcal{L}(\mathcal{D})$. \mathcal{L} tries to minimize the expected value of a supervised learning loss $l(\hat{f}(x), y) \in \mathbb{R}$ under unknown probability measure $P(Y|x)$. In this section, we focus on regression tasks with the squared loss $l(\hat{y}, y) = (\hat{y} - y)^2$, with $y \in \mathbb{R}$. In Appendix B, we provide the corresponding results for a general loss function, with discrete or continuous outputs.

Definition 1.1 *The expected loss of a predictor \hat{f} at x is defined as:*

$$\mathcal{U}(\hat{f}, x) = \int (\hat{f}(x) - y)^2 dP(y|x). \quad (1)$$

The expected loss is an unknown scalar, as we generally do not have access to the true data distribution $P(Y|x)$. The errors made by any predictor \hat{f} at x are due to both the inherent randomness of $P(Y|x)$ (aleatoric uncertainty) and the lack of knowledge of the predictor that can be tackled by acquiring more information around x (epistemic uncertainty). Because of this natural decomposition of the expected loss, we will also refer to it as **total uncertainty**, and we will use the two terms interchangeably.

Bayes-optimal predictors f^* satisfy the following equation at every x :

$$\forall \tilde{y} \in \mathbb{R} \quad \int (f^*(x) - y)^2 dP(y|x) \leq \int (\tilde{y} - y)^2 dP(y|x).$$

They depend on the underlying data distribution only and not on learner \mathcal{L} or trained predictor \hat{f} . Additionally, for any x , all Bayes-optimal predictors have the same total uncertainty at that x . The error made by a Bayes-optimal predictor is irreducible and we define it as the aleatoric uncertainty:

Definition 1.2 *The aleatoric uncertainty at x is the total uncertainty of any Bayes-optimal predictor f^* at x :*

$$\mathcal{A}(x) = \mathcal{U}(f^*, x). \quad (2)$$

and we note that by definition $\mathcal{A}(x) \leq \mathcal{U}(f, x)$, $\forall f \forall x$.

We now define the epistemic uncertainty of a predictor \hat{f} as the gap between the error of \hat{f} at x and the lowest possible error at x , i.e., the reducible part of the loss, given more knowledge.

Definition 1.3 *The epistemic uncertainty $\mathcal{E}(\hat{f}, x)$ of a predictor \hat{f} at x is given by*

$$\mathcal{E}(\hat{f}, x) = \mathcal{U}(\hat{f}, x) - \mathcal{A}(x) = \mathcal{U}(\hat{f}, x) - \mathcal{U}(f^*, x). \quad (3)$$

Using these definitions, we can present our main result for the regression setting.

Proposition 1 In a regression task with Gaussian ground truth $P(y|x) = \mathcal{N}(y; f^*(x), \sigma^2(x))$,

$$\begin{aligned}\mathcal{E}(\hat{f}, x) &= (\hat{f}(x) - f^*(x))^2 \\ \mathcal{U}(\hat{f}, x) &= \mathbb{E}_{P(y|x)}[(\hat{f}(x) - y)^2] = (\hat{f}(x) - f^*(x))^2 + \sigma^2(x) \\ \mathcal{A}(x) &= \mathbb{E}_{P(y|x)}[(f^*(x) - y)^2] = \sigma^2(x)\end{aligned}$$

The proof is provided in Appendix C.

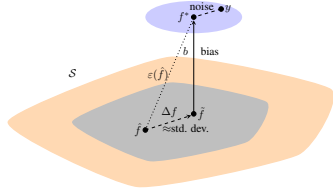


Figure 2: *Illustrating noise and bias. Observed y is independent noise plus true $\mathbb{E}[Y|x] = f^*(x)$, itself best approximated by unknown $\hat{f}(x)$ in parametric set S (orange), e.g., using Bayesian posterior distribution $p(f|\mathcal{D})$ (grey) over parameters. \hat{f} is the closest function in S to f^* , leading to a bias $b(x) = f^*(x) - \hat{f}(x)$. $\varepsilon(\hat{f})(x) = f^*(x) - \hat{f}(x)$ is the reducible error of the main predictor \hat{f} (e.g. posterior mean), whose square corresponds to EU or lack of knowledge, that DEUP aims at estimating. With \tilde{f} the unknown ideal predictor and \hat{f} the actual (e.g. mean) predictor, the square of $\Delta f(x) = \tilde{f}(x) - \hat{f}(x)$ induces variance in the posterior. $\varepsilon(\hat{f})(x) = b(x) + \Delta f(x)$ indicates that using the variance as a proxy for EU misses out a non-negligible quantity: the bias $b(x)$.*

tion properties of SGD [31], explicit regularization, early stopping or a combination of these, which can induce a preference on the functions it learns. In Fig. 2, we illustrate this gap with the bias function $b(x) = f^*(x) - \hat{f}(x)$. Because of this bias, model variance cannot be an accurate measure of EU $\mathcal{E}(\hat{f}, x)$ in the general case.

In Deep Ensembles [40], for example, if all the networks in the ensemble tend to fail in systematic (i.e. potentially reducible) ways, this aspect of prediction failure will not be captured by variance. Whereas Deep Ensembles variance provides us uncertainty regarding which of the networks we could draw is best, this does not tell us how poor that network is even in a noise-free setting. On the other hand, with flexible models like neural networks, adding examples around x where $b(x)^2$ is large may allow to increase capacity around x and reduce $b(x)^2$.

2 Direct Epistemic Uncertainty Prediction

DEUP (Direct Epistemic Uncertainty Prediction) **uses observed out-of-sample errors in order to train an error predictor which can be used to estimate epistemic uncertainty** elsewhere, as suggested directly by Def. 1.1-1.3. These may be in-distribution or out-of-distribution errors, depending on what we care about and the kind of data that is available. In Algo. 1, we provide the pseudo-code for DEUP in interactive settings. The pseudo-code for the simpler version with a fixed training set is given in Appendix D. We consider three separate cases for the aleatoric uncertainty:

1. If we know that $\mathcal{A}(x) = 0$ then $u(x)$ is an estimate of $\mathcal{E}(\hat{f}, x)$ as well as of $\mathcal{U}(\hat{f}, x)$. In this case, we choose a to be the zero function in Algo. 1. Example: Sec. 4.1. Also, in cases where it is not possible to estimate the aleatoric uncertainty, we can rely on the total uncertainty estimates as a proxy for EU. Example: Sec. 4.3.

Relation to existing notions of EU: Consider a parametric model $p(Y|x, \theta)$ and a learner maintaining a distribution over parameters $\theta \in \Theta$, each corresponding to a predictor f in a parametric set of functions S , possibly starting from a prior $p(\theta)$ that would lead to a posterior distribution $p(\theta|\mathcal{D})$. Clearly, the fact that multiple θ 's and corresponding values of f are compatible with the data and the prior indicates lack of knowledge. Because the lack of knowledge indicates where an interactive learner should acquire more information, this justifies the usage of dispersion measures, such as the variance or the entropy of the posterior predictive, as proxies for EU.

However, the limited capacity of S or the prior $p(\theta)$ may keep the optimal \tilde{f} in S at a distance from the Bayes-optimal predictor f^* . We can refer to these self-imposed constraints as a form of bias, in the sense that the learner is usually biased towards the prior preferences, e.g., towards smoother predictors (typically more so when the dataset is smaller). This arises when training neural networks with limited data, where the network may not use all of its capacity due to implicit (and not fully understood) regularization.

2. If an estimator $x \rightarrow a(x)$ of aleatoric uncertainty is available, then $u(x) - a(x)$ becomes an estimate of the epistemic uncertainty of \hat{f} at x . As an example for this scenario, consider an active learning setting, where the evaluation of a new candidate requires wet lab experiments, where we know the margins of errors of the instruments used.
3. When we have access to an oracle that samples Y given query x from the environment $P(Y|x)$ (e.g., in active learning or SMO), then $\mathcal{A}(x)$ can be estimated using the empirical variance of different outcomes of the oracle at the same input x ; see Appendix E. It is common practice to perform replicate experiments in biological assays [42, 64]. Variation across replicates, for a given input x , provides information about the amount of noise associated with x , i.e. the magnitude of the aleatoric uncertainty $\mathcal{A}(x)$.

2.1 Fixed Training Set

Consider the scenario with a fixed training set $\mathcal{D} = \{(x_i, y_i)\}_{i=1}^{N_{train}}$, where $x_i \sim P(X)$ and $y_i \sim P(Y|X = x_i) = \mathcal{N}(Y; f^*(x), \sigma^2(x))$. The goal is to obtain an estimator of the total uncertainty $\mathcal{U}(\hat{f}, \cdot)$ for $\hat{f} = \mathcal{L}(\mathcal{D})$, that can be readily applied for input points x sampled from the same distribution $P(X)$.

According to Prop.1, we can train a secondary predictor u on (input, target) pairs (x, e) , where $e = (y - \hat{f}(x))^2$ in order to obtain such an estimator. To see this, note that at the limit of infinite data, if the learning algorithm ensures asymptotic convergence to a Bayes-optimal predictor (such as k -nearest neighbors with k increasing at a proper rate, or neural networks whose size and regularization are hyperparameters optimized on a growing validation set), the resulting estimates $u(x)$ converge to $\mathbb{E}_{y \sim P(y|x)}[(\hat{f}(x) - y)^2] = \mathcal{U}(\hat{f}, x)$. These (input, target) pairs can be obtained from a hold-out dataset $\mathcal{D}^{OOS} = \{(x_i, y_i)\}_{i=N_{train}+1}^{N_{train}+N_{OOS}}$, sampled from the same distribution as \mathcal{D} .

2.2 Interactive Settings

Interactive settings, in which EU estimates are used to guide the acquisition of new examples, provide a more interesting use case for DEUP. They introduce however their own challenges, as the main predictor is retrained multiple times with the newly acquired points, which we address below.

We consider an initial training dataset $\mathcal{D}^0 = \{(x_i^0, y_i^0)\}_{i=1}^{N_0}$. At each round $t > 0$, we have access to a trained predictor \hat{f}^{t-1} , estimating the unknown ground-truth f^* , and an estimator \hat{e}^{t-1} of its EU. Suppose there is an acquisition function, that given any predictor \hat{f} and an estimator \hat{e} of its EU, defines a distribution on the input space \mathcal{X} : $\pi(X|\hat{f}, \hat{e})$, from which we can sample points to add to the training set. Assume that at round $t > 0$, N_t points $\{(x_i^t, y_i^t)\}_{i=1}^{N_t}$ are acquired, where $x_i^t \sim \pi(X|\hat{f}^{t-1}, \hat{e}^{t-1})$, and $y_i^t \sim P(Y|X = x_i^t) = \mathcal{N}(Y; f^*(x), \sigma^2(x))$ added to the training dataset: $\mathcal{D}^t = \mathcal{D}^{t-1} \cup \{(x_i^t, y_i^t)\}_{i=1}^{N_t}$. From \mathcal{D}^t , a predictor $\hat{f}^t = \mathcal{L}(\mathcal{D}^t)$ is obtained, which in turn will be used to decide which N_{t+1} points are going to be acquired next, through the acquisition policy π and an estimator \hat{e}^t of its EU. How can we train such an EU estimator, without wasting N_{OOS} (input, target) pairs that could be used to obtain a better estimator of f^* ?

Algorithm 1 Training procedure for DEUP in an Active Learning setting

Data: \mathcal{D}_{init} initial dataset with pairs $(x, y) \in \mathcal{X} \times \mathbb{R}$
 $a : \mathcal{X} \mapsto \mathbb{R}$, estimator of aleatoric uncertainty
 $\hat{f} : \mathcal{X} \mapsto \mathbb{R}$, main predictor (of y given x)
 $u : \mathcal{X} \mapsto \mathbb{R}$, total uncertainty estimator
 $\phi : \mathcal{X} \mapsto \mathbb{R}^k$, chosen stationarizing features
 π : acquisition machinery that proposes new input points from \mathcal{X} , using the current \hat{f} and EU estimates.
 $\mathcal{D}_u \leftarrow \emptyset$, training dataset for u
 $\mathcal{D} \leftarrow \mathcal{D}_{init}$, dataset of training points for \hat{f} seen so far
 $x_{acq} \leftarrow \emptyset, y_{acq} \leftarrow \emptyset$
Optional: Pre-fill \mathcal{D}_u using Algo. 2 and fit u on \mathcal{D}_u
while stopping criterion not reached **do**
 Optional: Fit a on \mathcal{D} if necessary (e.g. see Appendix E)
 Fit predictor \hat{f} and features ϕ on \mathcal{D}
 $\mathcal{D}_u \leftarrow \mathcal{D}_u \cup \{(\phi(x_{acq}), (y_{acq} - \hat{f}(x_{acq}))^2)\}$
 Fit u on \mathcal{D}_u
 $x_{acq} \sim \pi(\cdot | \hat{f}, u - a)$ (can be either a single point, or a batch of points)
 Sample outcomes from the ground truth distribution:
 $y_{acq} \sim P(\cdot | x_{acq})$
 $\mathcal{D}_u \leftarrow \mathcal{D}_u \cup \{(\phi(x_{acq}), (y_{acq} - \hat{f}(x_{acq}))^2)\}$
 $\mathcal{D} \leftarrow \mathcal{D} \cup \{(x_{acq}, y_{acq})\}$

end

The problem with the trivial dataset: Inspired by the fixed training set setting, it might be tempting to train an error predictor \hat{e}^t on $\mathcal{D}_{u,1}^t = \cup_{\tau=0}^t \{(x_i^\tau, (y_i^\tau - \hat{f}^t(x_i^\tau))^2)\}_{i=1}^{N_\tau}$. However, x_i^τ was used to train \hat{f}^t and so we have an in-sample rather than OOS error. There would thus be no reason for \hat{e}^t to provide accurate estimates in unexplored regions of the search space \mathcal{X} .

An alternative is to learn from the errors made by previous versions of the predictor, i.e. $\{f^\tau, \tau \in \{0, \dots, t\}\}$, on points that were not used to train each of them, which we can simply choose to be the subsequent acquired points. More formally, consider the dataset $\mathcal{D}_{u,2}^t = \cup_{\tau=0}^t \cup_{\tau'=\tau}^t \{(x_i^{\tau'}, (y_i^{\tau'} - \hat{f}^\tau(x_i^{\tau'}))^2)\}_{i=1}^{N_{\tau'}}$. A learning algorithm with good generalization properties (such as modern neural networks), would in principle be able to extrapolate from this dataset, and estimate the errors (or total uncertainty) made by \hat{f}^t on points $x \in \mathcal{X}$ not seen so far, i.e. belonging to what we call the *frontier of knowledge*. However, as each $x_i^{\tau'}$ appears $t - \tau' + 1$ times in $\mathcal{D}_{u,2}^t$, with different targets at each time (each corresponding to error made by \hat{f}^τ on $x_i^{\tau'}$, for $\tau \in \{\tau', \dots, t\}$), there is no reason to assume that the resulting predictor would estimate the errors of \hat{f}^t . The reason is that the targets are actually functions of not only the input x , but also of the dataset used to train the different predictors \hat{f}^τ , i.e. \mathcal{D}^τ . This is actually obvious when we write $(y_i^{\tau'} - \hat{f}^\tau(x_i^{\tau'}))^2 = \mathcal{U}(\mathcal{L}(\mathcal{D}^\tau), x_i^{\tau'})$. This means that in order to obtain an estimator \hat{e}^t , we should train a general error estimator \hat{e} , with inputs of the form (\mathcal{D}, x) and targets of the form $(y - \mathcal{L}(\mathcal{D})(x))^2$, using the historical dataset $\mathcal{D}_{u,2}^t = \cup_{\tau=0}^t \cup_{\tau'=\tau}^t \{((\mathcal{D}^\tau, x_i^{\tau'}), (y_i^{\tau'} - \hat{f}^\tau(x_i^{\tau'}))^2)\}_{i=1}^{N_{\tau'}}$, and then define $\hat{e}^t(x)$ to be $\hat{e}(\mathcal{D}^t, x)$ for any $x \in \mathcal{X}$. In summary, it is the acquired points, before they are added to the training set, that play the role of out-of-sample (they are actually OOD) points to train the EU estimator.

However, \mathcal{D} being a very high-dimensional object, with size growing with the number of acquired points, we may face severe overfitting issues when using (\mathcal{D}, x) as inputs. We thus propose using **stationarizing features** of the dataset \mathcal{D} at x , that we denote by $\phi_{\mathcal{D}}(x)$, as inputs to the error predictor instead of (\mathcal{D}, x) (we typically include x in $\phi_{\mathcal{D}}(x)$). These stationarizing features also address concerns with directly estimating uncertainty using a second order predictor trained simply using L2 error, raised in [8].

In this paper, we explored $\phi_{\mathcal{D}}(x) = (x, s, \hat{q}(x|\mathcal{D}), \hat{V}(\tilde{\mathcal{L}}, \mathcal{D}, x))$, where $\hat{q}(x|\mathcal{D})$ is a density estimate from data \mathcal{D} at x , $s = 1$ if $x \in \mathcal{D}$ otherwise 0, $\tilde{\mathcal{L}}$ a learner that produces a distribution over predictors, e.g. a GP or a Deep Ensemble [40]), and $\hat{V}(\tilde{\mathcal{L}}, \mathcal{D}, x)$ is an estimate of the model variance of $\tilde{\mathcal{L}}$ at x . Note that $\tilde{\mathcal{L}}$ can be chosen to be the same as \mathcal{L} . For numerical reasons, we found it preferable to use $\log \hat{q}$ and $\log \hat{V}$ instead of \hat{q} or \hat{V} as input features. \hat{q} can be obtained by training a density estimator (such as a Kernel Density Estimator or a flow-based deep network [63], in our case). Like the other predictors, the density estimator also needs to be fine-tuned when new data is added to the training set. While these features are not required per se to train DEUP, they provide clues to help training the uncertainty estimator, and one can play with the trade-off of computational cost versus usefulness of each clue. They sometimes come at no greater cost, if our main predictor is the mean prediction of the learner’s output distribution, and if we use the corresponding variance as the only extra feature, as is the case in the experiments of Sec. 4.1 with GPs.

In our experiments, we found that using inputs $\phi_{\mathcal{D}}(x)$, or even a subset of the 4 possible features, is sufficient to train an uncertainty estimator with targets $(\hat{f}(x) - y)^2$.

For computational reasons, it is unfeasible to store all previous datasets and all previous predictors \hat{f}^τ , and we propose a subset of $\mathcal{D}_{u,2}^t$, that makes it possible to have an online algorithm, without memorization:

$$\mathcal{D}_u^t = \cup_{\tau=0}^t \cup_{\tau'=\tau}^{\tau+1} \{(\phi_{\mathcal{D}^\tau}(x_i^{\tau'}), (y_i^{\tau'} - \hat{f}^\tau(x_i^{\tau'}))^2)\}_{i=1}^{N_{\tau'}}.$$

The corresponding pseudo-code is provided in Algo. 1. Note that \mathcal{D}_u is incremented twice with x_{acq} but $\phi_{\mathcal{D}}(x_{acq})$ is different each time because x_{acq} first is and then is not yet in \mathcal{D} .

2.2.1 Pretraining the error predictor

Consider an interactive setting, and suppose that the oracle is so costly that we cannot afford to wait for a few rounds of acquisition in order to build a training dataset large enough for the uncertainty estimator to provide reasonable EU estimates. To this end, we propose a cross-validation strategy to pretrain the secondary learner before any acquisition step, using pairs $(\phi_{\bar{\mathcal{D}}}(x), (f_{\bar{\mathcal{D}}}(x) - y)^2)$,

where \tilde{D} is any subset of the initially available data, that we use to train a predictor $f_{\tilde{D}} = \mathcal{L}(\tilde{D})$, and (x, y) any pair in D , whether in \tilde{D} or not. With this pretraining phase, we obtain better uncertainty estimates as soon as the first batch of acquired points come in. There are several ways to build the pretraining dataset. We present one of them in Alg. 2. The procedure stops when the training dataset for the secondary learner, \mathcal{D}_u , contains at least $N_{pretrain}$ elements. In our experiments, we choose $N_{pretrain}$ to be a small multiple of the number of initial training points.

Algorithm 2 Pre-filling the uncertainty estimator training dataset \mathcal{D}_u

Input: \mathcal{D}_u
while $|\mathcal{D}_u| < N_{pretrain}$ **do**
 Split \mathcal{D}_{init} into K random subsets $\mathcal{D}_1, \dots, \mathcal{D}_K$ of equal size. Define $\tilde{D} = \bigcup_{k=1}^{K-1} \mathcal{D}_k$
 Fit a new predictor \hat{f} on \tilde{D} , and fit the features ϕ on \tilde{D}
 $\mathcal{D}_u \leftarrow \mathcal{D}_u \cup \bigcup_{(x,y) \in \mathcal{D}} \{(\phi(x), (y - \hat{f}(x))^2)\}$
end

3 Related Work

In [35], the authors characterize the sources of uncertainty as aleatoric (inherent noise) and epistemic (incomplete knowledge). Using Gaussian Processes [79] or GP is a popular EU estimation because the variance among the functions in the posterior (given the data) can be computed analytically.

In a deep learning context, [9, 32, 16] use the posterior distribution of network weights [44] in Bayesian Neural Networks (BNNs) to capture EU. Other techniques that rely on measuring the discrepancy between different predictors as a proxy for EU include MC-Dropout [22], that interprets Dropout [26] as a variational inference technique in BNNs. These approaches, because they rely on sampling multiple sets of weights or dropout masks at inference time, share some similarities with ensemble-based methods, that include bagging [10] and boosting [18], in which multiple predictors are trained and their outputs are averaged to make a prediction, although the latter measure variability due to the training set instead of the spread of functions compatible with the given training set, as in Bayesian approaches. For example, [66] use Random Forests [11] to estimate EU. Deep Ensembles [40] are closer to the Bayesian approach, using an ensemble of neural networks that differ because of randomness in initialization and training (as you would have with MCMC, albeit in a more heuristic way). In addition to this, several other variants of this central idea of measuring discrepancy between different predictors have been proposed recently [47, 70, 3, 43, 76, 78, 4, 34, 46, 75, 55]. We discuss some of these methods in more detail in Appendix A.

More closely related to DEUP, [81] propose a loss prediction module for learning to predict the value of the loss function. [27] also propose using a separate network that learns to predict the variance of an ensemble. These methods, however, are trained only to capture the in-sample error, and do not capture the out-of-sample error which is more relevant for scenarios like active learning where we want to pick x where the reducible *generalization error* (see Def. 1.3) is large. EpiOut [72, 23] propose learning a binary output that simply distinguishes between low or high EU.

4 Experiments

In our experiments, we focus on interactive settings, where having good uncertainty estimates is essential for efficient acquisition. As explained in Sec. 2.2, it is the acquired points, before they are used to retrain the main predictor, that act as the *out-of-sample* examples to train DEUP. In RL, because the targets (e.g. of Q-Learning) are themselves estimates and moving, data seen at any particular point is normally out-of-sample and can inform the uncertainty estimator, when the inputs are used with the stationarizing features. We emphasize that in order to make fair comparisons, **DEUP does not have access to any additional OOD data during training**, in any of the experiments that follow. Instead, we use Algo. 2 to generate the OOD data used for training the error predictor. Finally, note that in terms of computational cost, training DEUP with density and model variance as stationarizing features is on-par with training an ensemble of 5 networks.

4.1 Sequential Model Optimization

Sequential model optimization is a form of active learning, where at each stage, the learner chooses query examples to label, looking for examples with a high value of the unknown oracle function. Such examples are selected so they have a high predicted value (to maximize the unknown oracle function) and a large predicted uncertainty (offering the opportunity of discovering yet higher values).

Acquisition functions, such as Upper Confidence Bound (UCB, [68]) and Expected Improvement (EI, [52]) trade-off exploration and exploitation, and one can select the next candidate by looking for x 's maximizing the acquisition function. We combine UCB and EI with DEUP (DEUP-UCB and DEUP-EI) to perform active learning, treating the main predictor and DEUP EU predictions at x respectively as mean and variance of a Gaussian distribution for the learner's guess of the value of the oracle at x . We showcase how using DEUP to calibrate GP variances (used as the only extra input for DEUP) allows for better performances in higher-dimensional optimization tasks. Specifically, we compare DEUP-EI to TuRBO-EI [19], a state-of-the-art method for sequential optimization, that fits a collection of local GP models instead of a global one in order to perform efficient high-dimensional optimization, on the Ackley function [1] as oracle, a common benchmark for optimization algorithms. The oracle function can be defined for arbitrary dimensions, and has many local minima.

In Fig. 3, we compare different methods on the Ackley-10 function, in addition to the optimum reached in budget-constrained optimization problems for different oracle input dimensions, and we find that adapting DEUP to TuRBO consistently outperforms regular TuRBO, especially in higher dimensions. See also Appendix F for 1D and 2D SMO tasks where DEUP-EI outperforms GP-EI [12], as well as neural networks with MC-Dropout or Ensembles. We find GP-EI getting stuck in local optima whereas DEUP-EI was able to reach the global maximum consistently. Experimental details are provided in Appendix F.3.

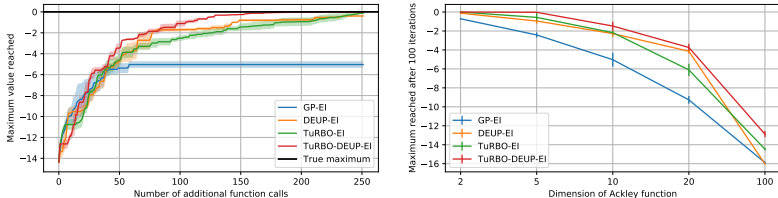


Figure 3: *Left*. Max. value reached by the different optimization methods, for the 10 dimensional Ackley function. In each run, all the methods start with the same initial 20 points. Shaded areas represent the standard error across 3 runs. *Right*. Max. value reached in the budget-constrained setting, on the Ackley functions of different dimensions. Error bars represent the standard error across 3 different runs, with different initial sets of 20 pairs. The budget is 120 function calls in total. Higher is better and TuRBO-DEUP-EI is less hurt by dimensionality.

4.2 Reinforcement Learning

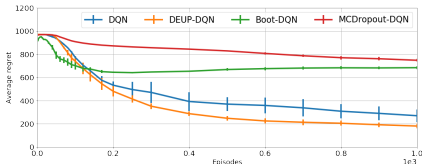


Figure 4: Average regret on CartPole task. Error bars represent standard error across 5 runs.

DEUP-DQN on CartPole, a classic RL task from *bsuite* [60], against DQN + ϵ -greedy, DQN + MC-Dropout [22] and Bootstrapped DQN [59]. Fig. 4 shows that DEUP achieves lower regret faster, compared to all the baselines, which demonstrates the advantage of DEUP's uncertainty estimates for efficient exploration. Future work should investigate ways to scale this method to more complex environments.

4.3 Uncertainty Estimation

4.3.1 Epistemic Uncertainty Predictions for Rejecting Difficult Examples

Epistemic uncertainty estimates can be used to reject difficult examples where the predictor might fail, such as OOD inputs². We thus consider a standard OOD Detection task [76, 75], where we train a ResNet-18 [24] for CIFAR-10 classification [37] and reject OOD examples using estimated uncertainty in the prediction. To facilitate rejection of classes other than those in the training set,

²e.g. rare but challenging inputs can be directed to a human, avoiding a costly mistake

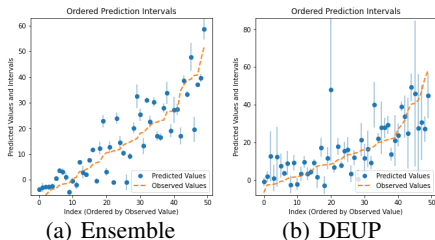
we use a Bernoulli Cross-Entropy Loss for each class [76]: $l(\hat{f}(x), y) = -\sum_i y_i \log \hat{f}_i(x) + (1 - y_i) \log(1 - \hat{f}_i(x))$, where y is a one-hot vector ($y_i = 1$ if i is the correct class, and 0 otherwise), and $\hat{f}_i(x) =$ predicted probability for class i , so the target for out-of-distribution data (from other classes) is $y = \{0, \dots, 0\}$. To ascertain how well an epistemic error estimate sorts non-training examples by the above NLL loss, we consider the rank correlation between the predicted uncertainty and the observed OOD generalization error on SVHN examples [56]. This metric focuses on the quality of the uncertainty estimates rather than just their ability to simply classify in- vs out-of-distribution. We also report the AUC for the OOD detection task; more details in Appendix H. Table 1 shows that with the variance from DUE [75] and the density from MAF [62] as stationarizing features, we obtain uncertainty estimates that have high rank correlation with the underlying generalization errors and competitive AUROC, compared with the baselines. In addition, since the error predictor is trained separately from the main predictor, there is no explicit trade-off between the accuracy of the main predictor and the quality of uncertainty estimates. We achieve competitive accuracy of 93.89% for the main predictor. We ignore the effect of aleatoric uncertainty (due to inconsistent human labelling), which would require a human study to ascertain. We note that we choose the DUE baseline as it is representative of related methods such as SNGP [43] and DDU [55], and performs best in our experiments. We present additional results in a distribution shift setting in Appendix H. Note that in the pretraining phase of the uncertainty estimator (Alg. 2), we obtain the subsets by splitting the data based on classes, with each split containing $\lfloor n/K \rfloor$ classes. So when we train on $K - 1$ subsets, the $\lfloor n/K \rfloor$ classes from the remaining subset become *out-of-distribution*.

Model	SRCC	AUROC
MC-Dropout	0.287 ± 0.002	0.894 ± 0.008
Deep Ensemble	0.381 ± 0.004	0.933 ± 0.008
DUQ	0.376 ± 0.003	0.927 ± 0.013
DUE	0.378 ± 0.004	0.929 ± 0.005
DEUP (D+V)	0.426 ± 0.009	0.933 ± 0.010

Table 1: Spearman Rank Correlation Coefficient (SRCC) between predicted uncertainty and OOD generalization error (SVHN); Area under ROC Curve (AUROC) for OOD Detection (SVHN) with CIFAR-10 ResNet-18 models (3 seeds). DEUP significantly outperforms baselines in terms of SRCC and is equivalent to Deep Ensembles but scoring better than the other methods in terms of the coarser AUROC metric.

This metric focuses on the quality of the uncertainty estimates rather than just their ability to simply classify in- vs out-of-distribution. We also report the AUC for the OOD detection task; more details in Appendix H. Table 1 shows that with the variance from DUE [75] and the density from MAF [62] as stationarizing features, we obtain uncertainty estimates that have high rank correlation with the underlying generalization errors and competitive AUROC, compared with the baselines. In addition, since the error predictor is trained separately from the main predictor, there is no explicit trade-off between the accuracy of the main predictor and the quality of uncertainty estimates. We achieve competitive accuracy of 93.89% for the main predictor. We ignore the effect of aleatoric uncertainty (due to inconsistent human labelling), which would require a human study to ascertain. We note that we choose the DUE baseline as it is representative of related methods such as SNGP [43] and DDU [55], and performs best in our experiments. We present additional results in a distribution shift setting in Appendix H. Note that in the pretraining phase of the uncertainty estimator (Alg. 2), we obtain the subsets by splitting the data based on classes, with each split containing $\lfloor n/K \rfloor$ classes. So when we train on $K - 1$ subsets, the $\lfloor n/K \rfloor$ classes from the remaining subset become *out-of-distribution*.

4.3.2 Epistemic Uncertainty Estimation for Drug Combinations



Model	Corr. w. res.	U. Bound	Ratio	Log Likelihood
MC-Dropout	0.14 ± 0.07	0.56 ± 0.05	0.25 ± 0.12	-20.1 ± 6.8
Deep Ensemble	0.30 ± 0.09	0.59 ± 0.04	0.50 ± 0.13	-14.3 ± 4.7
DUE	0.12 ± 0.12	0.15 ± 0.03	0.80 ± 0.79	-13.0 ± 0.52
DEUP	0.47 ± 0.03	0.63 ± 0.05	0.75 ± 0.07	-3.5 ± 0.25

(c) Quality of uncertainty estimates from different methods.

Figure 5: Drug Combinations. Predicted mean and uncertainty (error bars) on 50 test examples ordered by increasing value of true synergy score (orange). Model predictions and uncertainties in blue. Ensemble (a) (and MC-dropout, not shown) consistently underestimate uncertainty while DEUP (b) captures the right order of magnitude. (c) *Corr. w. res.* shows correlation between model residuals and predicted uncertainties $\hat{\sigma}$. A best-case *Upper Bound* on *Corr. w. res.* is obtained from the correlation between $\hat{\sigma}$ and true samples from $\mathcal{N}(0, \hat{\sigma})$. *Ratio* is the ratio between col. 1 and 2 (larger is better). *Log-likelihood*: average over 3 seeds of per sample predictive log-likelihood.

We validate DEUP in a real-world regression task predicting the synergy of drug combinations. While much effort in drug discovery is spent on finding novel small molecules, a potentially cheaper method is identifying combinations of pre-existing drugs which are synergistic (i.e., work well together). However, every possible combination cannot be tested due to the high monetary cost and time required to run experiments. Therefore, developing good estimates of EU can help practitioners select experiments that are both informative and promising. As shown in Table 5(c), the out-of-sample error predicted by DEUP correlates better with residuals of the model on the test set in comparison

to several other uncertainty estimation methods. Moreover, DEUP better captured the order of magnitude of the residuals as shown in Fig. 5. Details on experiments and metrics are in Appendix I.

5 Conclusion and Future Work

Whereas standard measures of epistemic uncertainty focus on variance, we argue that bias (misspecification) can also be reduced with predictors like neural networks. In a regression setup, the expected out-of-sample squared error minus aleatoric uncertainty thus captures all the uncertainty about the ground-truth function $\mathbb{E}[Y|x]$, that more data can reduce. This motivates the DEUP framework, where we train a second network to predict the errors of the first. In interactive settings, this nonetheless raises non-stationarity challenges for this estimator, and we propose extra input features to tackle this issue, and show experimentally their advantages. Future work should investigate ways to improve the computational efficiency of DEUP, and ways to estimate aleatoric uncertainty when no estimator thereof is readily available and when one cannot simply query an oracle several times on the same input x .

Acknowledgements

The authors would like to thank Tristan Deleu, Anirudh Goyal, Tom Bosc, Léna Néhale Ezzine, Doina Precup, Pierre Luc-Bacon, John Bradshaw, José Miguel Hernández-Lobato as well as anonymous reviewers for useful comments and feedback. This research was enabled in part by support provided by [Compute Canada](#), the Bill & Melinda Gates Foundation, IVADO and a CIFAR AI Chair. The authors also acknowledge funding from Samsung, IBM, Microsoft.

References

- [1] D. Ackley. *A connectionist machine for genetic hillclimbing*, volume 28. Springer Science & Business Media, 2012.
- [2] C. C. Aggarwal, X. Kong, Q. Gu, J. Han, and S. Y. Philip. Active learning: A survey. In *Data Classification: Algorithms and Applications*, pages 571–605. CRC Press, 2014.
- [3] A. Amini, W. Schwarting, A. Soleimany, and D. Rus. Deep evidential regression. In *Neural Information Processing Systems (NeurIPS)*, 2020.
- [4] J. Antoran, J. Allingham, and J. M. Hernández-Lobato. Depth uncertainty in neural networks. In *Neural Information Processing Systems (NeurIPS)*, 2020.
- [5] M. Balandat, B. Karrer, D. R. Jiang, S. Daulton, B. Letham, A. G. Wilson, and E. Bakshy. BoTorch: A Framework for Efficient Monte-Carlo Bayesian Optimization. In *Advances in Neural Information Processing Systems 33*, 2020.
- [6] P. J. Ballester and J. B. Mitchell. A machine learning approach to predicting protein–ligand binding affinity with applications to molecular docking. *Bioinformatics*, 26(9):1169–1175, 2010.
- [7] E. Bengio, M. Jain, M. Korablyov, D. Precup, and Y. Bengio. Flow network based generative models for non-iterative diverse candidate generation. *NeurIPS’2021*, *arXiv:2106.04399*, 2021.
- [8] V. Bengs, E. Hüllermeier, and W. Waegeman. On the difficulty of epistemic uncertainty quantification in machine learning: The case of direct uncertainty estimation through loss minimisation. *arXiv preprint arXiv:2203.06102*, 2022.
- [9] C. Blundell, J. Cornebise, K. Kavukcuoglu, and D. Wierstra. Weight uncertainty in neural network. In *International Conference on Machine Learning*, pages 1613–1622. PMLR, 2015.
- [10] L. Breiman. Bagging predictors. *Machine learning*, 24(2):123–140, 1996.
- [11] L. Breiman. Random forests. *Machine learning*, 45(1):5–32, 2001.
- [12] A. D. Bull. Convergence rates of efficient global optimization algorithms. *Journal of Machine Learning Research*, 12(10), 2011.
- [13] M. R. Cervera, R. Dätwyler, F. D’Angelo, H. Keurti, B. F. Grewe, and C. Henning. Uncertainty estimation under model misspecification in neural network regression, 2021.

- [14] Y. Chung, W. Neiswanger, I. Char, and J. Schneider. Beyond pinball loss: Quantile methods for calibrated uncertainty quantification. *arXiv preprint arXiv:2011.09588*, 2020.
- [15] T. Cihlar and M. Fordyce. Current status and prospects of hiv treatment. *Current opinion in virology*, 18:50–56, 2016.
- [16] S. Depeweg, J.-M. Hernandez-Lobato, F. Doshi-Velez, and S. Udluft. Decomposition of uncertainty in bayesian deep learning for efficient and risk-sensitive learning. In *International Conference on Machine Learning*, pages 1184–1193. PMLR, 2018.
- [17] M. W. Dusenberry, G. Jerfel, Y. Wen, Y. Ma, J. Snoek, K. Heller, B. Lakshminarayanan, and D. Tran. Efficient and scalable bayesian neural nets with rank-1 factors. In *International Conference on Machine Learning (ICML)*, 2020.
- [18] B. Efron and R. J. Tibshirani. *An introduction to the bootstrap*. CRC press, 1994.
- [19] D. Eriksson, M. Pearce, J. R. Gardner, R. Turner, and M. Poloczek. Scalable global optimization via local bayesian optimization. *arXiv preprint arXiv:1910.01739*, 2019.
- [20] S. Farquhar, Y. Gal, and T. Rainforth. On statistical bias in active learning: How and when to fix it. *ICLR’2021, arXiv:2101.11665*, 2021.
- [21] P. Frazier. A tutorial on bayesian optimization. *ArXiv*, abs/1807.02811, 2018.
- [22] Y. Gal and Z. Ghahramani. Dropout as a bayesian approximation: Representing model uncertainty in deep learning. In *International Conference on Machine Learning (ICML)*, pages 1050–1059. PMLR, 2016.
- [23] D. Hafner, D. Tran, T. Lillicrap, A. Irpan, and J. Davidson. Noise contrastive priors for functional uncertainty. In *Conference on Uncertainty in Artificial Intelligence (UAI)*, 2019.
- [24] K. He, X. Zhang, S. Ren, and J. Sun. Deep residual learning for image recognition. In *Proceedings of the IEEE conference on computer vision and pattern recognition*, pages 770–778, 2016.
- [25] D. Hendrycks and T. Dietterich. Benchmarking neural network robustness to common corruptions and perturbations. *Proceedings of the International Conference on Learning Representations*, 2019.
- [26] G. E. Hinton, N. Srivastava, A. Krizhevsky, I. Sutskever, and R. R. Salakhutdinov. Improving neural networks by preventing co-adaptation of feature detectors. *arXiv preprint arXiv:1207.0580*, 2012.
- [27] S. Hu, N. Pezzotti, and M. Welling. A new perspective on uncertainty quantification of deep ensembles. *arXiv*, 2020.
- [28] P. Izmailov, D. Podoprikin, T. Garipov, D. Vetrov, and A. Wilson. Averaging weights leads to wider optima and better generalization. In *Conference on Uncertainty in Artificial Intelligence (UAI)*, 2018.
- [29] D. Janz, J. Hron, P. Mazur, K. Hofmann, J. M. Hernández-Lobato, and S. Tschiatschek. Successor uncertainties: Exploration and uncertainty in temporal difference learning. In *Neural Information Processing Systems (NeurIPS)*, 2019.
- [30] D. R. Jones, M. Schonlau, and W. J. Welch. Efficient global optimization of expensive black-box functions. *Journal of Global optimization*, 13(4):455–492, 1998.
- [31] S. Kale, A. Sekhari, and K. Sridharan. Sgd: The role of implicit regularization, batch-size and multiple-epochs. In *NeurIPS*, 2021.
- [32] A. Kendall and Y. Gal. What uncertainties do we need in bayesian deep learning for computer vision? In *Neural Information Processing Systems (NeurIPS)*, 2017.
- [33] D. P. Kingma and J. Ba. Adam: A method for stochastic optimization. In *International Conference for Learning Representations*, 2015.
- [34] P. Kirichenko, P. Izmailov, and A. G. Wilson. Why normalizing flows fail to detect out-of-distribution data. In *Neural Information Processing Systems (NeurIPS)*, 2020.
- [35] A. D. Kiureghian and O. Ditlevsen. Aleatory or epistemic? does it matter? *Structural Safety*, 31(2):105–112, 2009. Risk Acceptance and Risk Communication.
- [36] L. Kocsis and C. Szepesvári. Bandit based monte-carlo planning. In *In: ECML-06. Number 4212 in LNCS*, pages 282–293. Springer, 2006.

- [37] A. Krizhevsky. Learning multiple layers of features from tiny images. Technical report, University of Toronto, 2009.
- [38] M. Kull and P. Flach. Novel decompositions of proper scoring rules for classification: Score adjustment as precursor to calibration. In *Machine Learning and Knowledge Discovery in Databases*, 2015.
- [39] H. J. Kushner. A new method of locating the maximum point of an arbitrary multipeak curve in the presence of noise. *Journal of Basic Engineering*, 86:97–106, 1964.
- [40] B. Lakshminarayanan, A. Pritzel, and C. Blundell. Simple and scalable predictive uncertainty estimation using deep ensembles. In *Neural Information Processing Systems (NeurIPS)*, 2017.
- [41] Y. LeCun, L. Bottou, Y. Bengio, and P. Haffner. Gradient-based learning applied to document recognition. *Proceedings of the IEEE*, 86(11):2278–2324, 1998.
- [42] M.-L. T. Lee, F. C. Kuo, G. Whitmore, and J. Sklar. Importance of replication in microarray gene expression studies: statistical methods and evidence from repetitive cDNA hybridizations. *Proceedings of the National Academy of Sciences*, 97(18):9834–9839, 2000.
- [43] J. Z. Liu, Z. Lin, S. Padhy, D. Tran, T. Bedrax-Weiss, and B. Lakshminarayanan. Simple and principled uncertainty estimation with deterministic deep learning via distance awareness. In *Neural Information Processing Systems (NeurIPS)*, 2020.
- [44] D. J. MacKay. A practical bayesian framework for backpropagation networks. *Neural computation*, 4(3):448–472, 1992.
- [45] W. Maddox, T. Garipov, P. Izmailov, D. Vetrov, and A. G. Wilson. A simple baseline for bayesian uncertainty in deep learning. In *Neural Information Processing Systems (NeurIPS)*, 2019.
- [46] A. Malinin, S. Chervontsev, I. Provilkov, and M. Gales. Regression prior networks, 2020.
- [47] A. Malinin and M. Gales. Predictive uncertainty estimation via prior networks. In *NIPS’18: Proceedings of the 32nd International Conference on Neural Information Processing Systems*, 2018.
- [48] A. Malinin, B. Mlodozieniec, and M. Gales. Ensemble distribution distillation. In *International Conference on Learning Representations*, 2020.
- [49] A. Malyutina, M. M. Majumder, W. Wang, A. Pessia, C. A. Heckman, and J. Tang. Drug combination sensitivity scoring facilitates the discovery of synergistic and efficacious drug combinations in cancer. *PLoS computational biology*, 15(5):e1006752, 2019.
- [50] A. Masegosa. Learning under model misspecification: Applications to variational and ensemble methods. In H. Larochelle, M. Ranzato, R. Hadsell, M. F. Balcan, and H. Lin, editors, *Advances in Neural Information Processing Systems*, 2020.
- [51] V. Mnih, K. Kavukcuoglu, D. Silver, A. Graves, I. Antonoglou, D. Wierstra, and M. Riedmiller. Playing atari with deep reinforcement learning. *arXiv preprint arXiv:1312.5602*, 2013.
- [52] J. Moćkus. On bayesian methods for seeking the extremum. In *Optimization techniques IFIP technical conference*, pages 400–404. Springer, 1975.
- [53] R. B. Mokhtari, T. S. Homayouni, N. Baluch, E. Morgatskaya, S. Kumar, B. Das, and H. Yeger. Combination therapy in combating cancer. *Oncotarget*, 8(23):38022, 2017.
- [54] H. L. Morgan. The generation of a unique machine description for chemical structures—a technique developed at chemical abstracts service. *Journal of Chemical Documentation*, 5(2):107–113, 1965.
- [55] J. Mukhoti, A. Kirsch, J. van Amersfoort, P. H. S. Torr, and Y. Gal. Deep deterministic uncertainty: A simple baseline, 2021.
- [56] Y. Netzer, T. Wang, A. Coates, A. Bissacco, B. Wu, and A. Y. Ng. Reading digits in natural images with unsupervised feature learning. In *Advances in Neural Information Processing Systems (NIPS)*, 2011.
- [57] V.-L. Nguyen, S. Destercke, and E. Hüllermeier. Epistemic uncertainty sampling. In *International Conference on Discovery Science*, pages 72–86. Springer, 2019.
- [58] W. H. Organization and S. T. Initiative. *Treatment of tuberculosis: guidelines*. World Health Organization, 2010.

- [59] I. Osband, C. Blundell, A. Pritzel, and B. Van Roy. Deep exploration via bootstrapped dqn. *arXiv preprint arXiv:1602.04621*, 2016.
- [60] I. Osband, Y. Doron, M. Hessel, J. Aslanides, E. Sezener, A. Saraiva, K. McKinney, T. Lattimore, C. Szepesvári, S. Singh, B. Van Roy, R. Sutton, D. Silver, and H. van Hasselt. Behaviour suite for reinforcement learning. In *International Conference on Learning Representations*, 2020.
- [61] Y. Ovadia, E. Fertig, J. Ren, Z. Nado, D. Sculley, S. Nowozin, J. Dillon, B. Lakshminarayanan, and J. Snoek. Can you trust your model's uncertainty? evaluating predictive uncertainty under dataset shift. In *Advances in Neural Information Processing Systems*, 2019.
- [62] G. Papamakarios, T. Pavlakou, and I. Murray. Masked autoregressive flow for density estimation. In *Neural Information Processing Systems (NeurIPS)*, 2017.
- [63] D. Rezende and S. Mohamed. Variational inference with normalizing flows. In *International Conference on Machine Learning (ICML)*, pages 1530–1538. PMLR, 2015.
- [64] N. J. Schurch, P. Schofield, M. Gierliński, C. Cole, A. Sherstnev, V. Singh, N. Wrobel, K. Gharbi, G. G. Simpson, T. Owen-Hughes, et al. How many biological replicates are needed in an rna-seq experiment and which differential expression tool should you use? *Rna*, 22(6):839–851, 2016.
- [65] M. Sensoy, L. Kaplan, and M. Kandemir. Evidential deep learning to quantify classification uncertainty. In *Neural Information Processing Systems (NeurIPS)*, page 3183–3193, 2018.
- [66] M. H. Shaker and E. Hüllermeier. Aleatoric and epistemic uncertainty with random forests. In *International Symposium on Intelligent Data Analysis*, pages 444–456. Springer, 2020.
- [67] J. Snoek, H. Larochelle, and R. P. Adams. Practical bayesian optimization of machine learning algorithms. In *Neural Information Processing Systems (NeurIPS)*, 2012.
- [68] N. Srinivas, A. Krause, S. M. Kakade, and M. Seeger. Gaussian process optimization in the bandit setting: No regret and experimental design. In *International Conference on Machine Learning (ICML)*, 2010.
- [69] A. Subramanian, R. Narayan, S. M. Corsello, D. D. Peck, T. E. Natoli, X. Lu, J. Gould, J. F. Davis, A. A. Tubelli, J. K. Asiedu, et al. A next generation connectivity map: L1000 platform and the first 1,000,000 profiles. *Cell*, 171(6):1437–1452, 2017.
- [70] N. Tagasovska and D. Lopez-Paz. Single-model uncertainties for deep learning. In *Neural Information Processing Systems (NeurIPS)*, 2019.
- [71] H. Tang, R. Houthoofd, D. Foote, A. Stooke, X. Chen, Y. Duan, J. Schulman, F. De Turck, and P. Abbeel. # exploration: A study of count-based exploration for deep reinforcement learning. In *Neural Information Processing Systems (NeurIPS)*, 2017.
- [72] J. Umlauf, A. Lederer, T. Beckers, and S. Hirche. Real-time uncertainty decomposition for online learning control. *ArXiv*, abs/2010.02613, 2020.
- [73] M. P. Vadera, A. D. Cobb, B. Jalaeian, and B. M. Marlin. Ursabench: Comprehensive benchmarking of approximate bayesian inference methods for deep neural networks. *ArXiv*, abs/2007.04466, 2020.
- [74] M. P. Vadera, B. Jalaeian, and B. M. Marlin. Generalized bayesian posterior expectation distillation for deep neural networks. In *UAI*, 2020.
- [75] J. van Amersfoort, L. Smith, A. Jesson, O. Key, and Y. Gal. Improving deterministic uncertainty estimation in deep learning for classification and regression. *CoRR*, abs/2102.11409, 2021.
- [76] J. R. van Amersfoort, L. Smith, Y. Teh, and Y. Gal. Simple and scalable epistemic uncertainty estimation using a single deep deterministic neural network. In *International Conference on Machine Learning (ICML)*, 2020.
- [77] M. Welling and Y. W. Teh. Bayesian learning via stochastic gradient langevin dynamics. In *Proceedings of the 28th International Conference on International Conference on Machine Learning*, 2011.
- [78] Y. Wen, D. Tran, and J. Ba. Batchensemble: An alternative approach to efficient ensemble and lifelong learning. In *International Conference on Learning Representations*, 2020.
- [79] C. K. Williams and C. Rasmussen. Gaussian processes for regression. In *Neural Information Processing Systems (NeurIPS)*, 1995.

- [80] A. G. Wilson, Z. Hu, R. Salakhutdinov, and E. P. Xing. Deep kernel learning. In A. Gretton and C. C. Robert, editors, *Proceedings of the 19th International Conference on Artificial Intelligence and Statistics (AISTATS)*, volume 51 of *Proceedings of Machine Learning Research*, pages 370–378, Cadiz, Spain, 09–11 May 2016. PMLR.
- [81] D. Yoo and I. Kweon. Learning loss for active learning. *2019 IEEE/CVF Conference on Computer Vision and Pattern Recognition (CVPR)*, pages 93–102, 2019.
- [82] B. Zagidullin, J. Aldahdooh, S. Zheng, W. Wang, Y. Wang, J. Saad, A. Malyutina, M. Jafari, Z. Tanoli, A. Pessia, et al. Drugcomb: an integrative cancer drug combination data portal. *Nucleic acids research*, 47(W1):W43–W51, 2019.
- [83] R. Zhang, C. Li, J. Zhang, C. Chen, and A. G. Wilson. Cyclical stochastic gradient mcmc for bayesian deep learning. In *ICLR*, 2020.
- [84] S. Zhang, A. Golbraikh, S. Oloff, H. Kohn, and A. Tropsha. A novel automated lazy learning qsar (all-qsar) approach: method development, applications, and virtual screening of chemical databases using validated all-qsar models. *Journal of chemical information and modeling*, 46(5):1984–1995, 2006.

Appendices

A Related Work

Recently, several novel deep learning-based techniques to estimate uncertainty with a single model have been proposed. For example, Deep Evidential Regression [3] is a method for estimating epistemic uncertainty that is based on a parametric estimate of model variance. This is in line with previous work using evidential uncertainty estimation [47, 65]. Orthonormal Certificates, a set of learned features with a suitable loss function, are used in [70]. These certificates capture the distance to the training set to learn an estimate of the epistemic uncertainty. This is further studied in [43] who formalize *distance awareness*, which captures the model’s ability to quantify the distance of a test sample from the training data manifold, as a necessary condition for uncertainty estimation. This distance awareness can be captured with a weight normalization step in training, in addition to using a GP as the output layer. DUE [75] is an instance of Deep Kernel Learning [80], which is defined as a GP with a deep feature extractor inside the kernel. DUE improves upon SNGP by using an inducing point GP, and bi-lipschitz constraints on the feature extractor, giving better test set accuracies as well as improved training efficiency. DDU [55] further extends this line of work by fitting Gaussian Discriminant Analysis (GDA) on the feature space of a regularized neural network. DUN [4] uses the disagreement between the outputs from intermediate layers as a measure of uncertainty. DUQ [76] on the other hand uses two-sided Jacobian regularization on RBF networks [41] for reliable uncertainty estimates.

[78] present an efficient way of implementing ensembles of neural networks, by using one shared matrix and a rank-1 matrix per member. The weights for each member are then computed as the Hadamard product of the shared matrix and the rank-1 matrix of the member. There has also been extensive work in scaling up Bayesian Neural Networks for high-dimensional data to capture epistemic uncertainty. SWAG [45] fits a Gaussian distribution capturing the SWA [28] mean and a covariance matrix representing the first two moments of SGD iterated. This distribution is then used as a posterior over the neural network weights. [17] parametrize the BNN with a distribution on a rank-1 subspace for each weight matrix, inspired by BatchEnsembles [78]. [74, 48] propose approaches to improve the efficiency of ensembles by distilling the distribution of predictions rather than the average, thus preserving the information about the uncertainty captured by the ensemble.

There is also a large body of work on methods for approximating samples from the Bayesian posterior on large datasets with efficient MCMC based approaches. [77, 83, 73]. The variance of this posterior distribution can then be computed and used as an uncertainty estimate. However, as we have discussed in the sections above, this does not account for model misspecification and thus is not an accurate estimate for the lack of knowledge of the predictor.

[38] present several decompositions of the total expected loss, including the decomposition into the epistemic and irreducible (aleatoric) loss. They present additive adjustments that reduce the scoring rules like the log-loss and Brier score, but do not tackle the general problem of uncertainty estimation.

There are also interesting connections between the problem of out-of-distribution generalization arising in sequential model optimization and Bayesian optimization, discussed here, and the possibility of reweighing examples, see [20].

B Epistemic Uncertainty in a general loss function setting

We consider the setting presented in section 1, but with a general loss function l . We use the same notations as in section 1.

Definition B.1 *The total uncertainty of f at x is defined as:*

$$U(f, x) = \int l(f(x), y) dP(y|x). \quad (4)$$

Definition B.2 *For a learning algorithm \mathcal{L} which produces a distribution $P_{\mathcal{L}}(f(x)|\mathcal{D}_n)$ over possible solutions $f(x)$ at x , the model variance at x is defined as*

$$V(\mathcal{L}, \mathcal{D}_n, x) = \int l(f(x), \hat{f}(x)) dP_{\mathcal{L}}(f(x)|\mathcal{D}_n) \quad (5)$$

with $\hat{f}(x) = \arg \min_{\bar{f}(x)} \int l(f(x), \bar{f}(x)) dP_{\mathcal{L}}(f(x)|\mathcal{D}_n)$. Note that for a loss function that is different from the square loss, the semantics of variance (such as its non-negativity) might be lost.

Let us consider the special cases of the negative log-likelihood loss in general (for outputs which may be discrete or continuous) and that of the squared error loss (which ends up being a special case of the former for normally distributed outputs). Below we see $Q(Y|x)$ as a probability mass or density function (over y), which is also a function of x .

Definition B.3 The negative log-likelihood (NLL) loss takes as first argument $Q(Y|x)$ a probability mass or density function and returns

$$l_{NLL}(Q(Y|x), y) = -\log Q(Y = y|x). \quad (6)$$

Proposition 2 For the NLL loss with ground truth $P(Y|x)$ and predictor $Q(Y|x)$, the total uncertainty $\mathcal{U}(Q(Y|x), x)$ is a cross-entropy, i.e.,

$$\begin{aligned} \mathcal{U}(Q(Y|\cdot), x) &= CE(P(Y|x)||Q(Y|x)) \\ &= -\int dP(y|x) \log Q(y|x) \end{aligned} \quad (7)$$

The proposition is shown by applying the definitions.

Proposition 3 For the NLL loss with ground truth $P(Y|x)$, the aleatoric uncertainty $\mathcal{A}(x)$ in this setting is the entropy $H[P(Y|x)]$ of the ground truth conditional:

$$\mathcal{A}(x) = -\int dP(y|x) \log P(y|x) = H[P(Y|x)], \quad (8)$$

The proposition is shown from the cross-entropy $CE(P(Y|x)||Q(Y|x))$ being minimized when $Q = P$.

Proposition 4 For the NLL loss with ground truth $P(Y|x)$ and predictor $Q(Y|x)$, the epistemic uncertainty $\mathcal{E}(Q(Y|x), x)$ is the Kullback-Liebler divergence between P and Q (with P as the reference):

$$\begin{aligned} \mathcal{E}(Q(Y|\cdot), x) &= KL(P(Y|x)||Q(Y|x)) \\ &= \int dP(y|x) \log \frac{P(y|x)}{Q(y|x)} \end{aligned} \quad (9)$$

The proposition is shown by combining the above two propositions and the definition of epistemic uncertainty.

To move towards the MSE loss, consider the special case of NLL with a conditionally Normal output density for both P and Q .

Proposition 5 For the NLL loss with a conditionally Normal output density for both P and Q , with respective means $f^*(x)$ and $\hat{f}(x)$ and respective variances $\sigma_P^2(x)$ and $\sigma_Q^2(x)$, the epistemic uncertainty is

$$\mathcal{E}(Q(Y|\cdot), x) = \frac{1}{2\sigma_Q^2(x)} l_{MSE}(\hat{f}(x), f^*(x)) + KL(P(Y|x)||\tilde{Q}(Y|x)), \quad (10)$$

where $\tilde{Q}(\cdot|x)$ is obtained by shifting $Q(\cdot|x)$ towards $P(\cdot|x)$ (i.e., $\tilde{Q}(\cdot|x)$ is Gaussian with mean $f^*(x)$ and variance $\sigma_Q^2(x)$), and the Bayes-optimal mean predictor is $f^*(x) = E_P[Y|x]$. Note that if $\sigma_P = \sigma_Q$, then the KL term is zero.

The proof is presented in Appendix C. We can compare with the MSE loss (which assumes a constant variance $\sigma = \sigma_P = \sigma_Q$) and obtain the same result up to variance scaling.

C Proofs

C.1 Proposition 1

It is a well known result that, because $f^*(x)$ is the mean of $P(\cdot|x)$, it is also the minimizer of $\hat{y} \mapsto \int (\hat{y} - y)^2 dP(y|x)$. f^* is thus a Bayes Optimal predictor.

By definition of the total uncertainty:

$$\mathcal{U}(f, x) = \int (f(x) - y)^2 dP(y|x) = E[(f(x) - Y)^2].$$

Hence, by definition of aleatoric uncertainty:

$$\mathcal{A}(x) = \mathcal{U}(f^*, x) = E[(f^*(x) - Y)^2].$$

and by definition of epistemic uncertainty

$$\begin{aligned} \mathcal{E}(f, x) &= E[(f(x) - y)^2 - (f^*(x) - y)^2] \\ &= f(x)^2 - f^*(x)^2 - 2(f(x) - f^*(x))f^*(x) \\ &= (f(x) - f^*(x))^2. \end{aligned}$$

Which concludes the proof.

C.2 Proposition 5

From Equation 9, we get:

$$\begin{aligned} \mathcal{E}(Q(Y|\cdot), x) &= KL(P(Y|x)||Q(Y|x)) \\ &= \log \frac{\sigma_Q(x)}{\sigma_P(x)} + \frac{\sigma_P^2(x) + (f(x) - f^*(x))^2}{2\sigma_Q^2(x)} - \frac{1}{2} \\ &= \frac{1}{2\sigma_Q^2(x)} l_{MSE}(f(x), f^*(x)) + \log \frac{\sigma_Q(x)}{\sigma_P(x)} + \frac{\sigma_P^2(x) + (f^*(x) - f^*(x))^2}{2\sigma_Q^2(x)} - \frac{1}{2} \\ &= \frac{1}{2\sigma_Q^2(x)} l_{MSE}(f(x), f^*(x)) + KL(P(Y|x)|\tilde{Q}(Y|x)) \end{aligned}$$

Which concludes the proof

D Pseudo Code for the fixed training set setting

Algorithm 3 illustrates the training procedure when a held-out validation set is available. We focus on $y \in \mathbb{R}$ in this paper because it makes sense for active learning applied to black-box optimization (where we want to maximize it) but the algorithms can trivially be applied to the case where $y \in \mathbb{R}^d$ for any d . Similarly, the algorithms can be generalized to other losses besides the square loss, following the generalized theory presented above in Appendix B.

E Estimating Aleatoric Uncertainty with access to an oracle

In scenarios like active learning, one has access to an oracle from which we can obtain samples of $Y \sim P(Y|x)$ at any given point x . In that case, one can train an estimator $a(x)$ of aleatoric uncertainty by obtaining $K > 1$ samples y_1, \dots, y_K at the same x , for a set of representative x 's.

More formally, if we have multiple independent outcomes $y_1, \dots, y_K \sim P(Y|x)$ for each input point x , then training a predictor a with the squared loss on (input, target) examples $\left(x, \frac{K}{K-1} \overline{Var}(y_1, \dots, y_K)\right)$, where \overline{Var} denotes the empirical variance, yields an estimator of the aleatoric uncertainty.

Naturally, this estimator is asymptotically unbiased, if the learning algorithm ensures asymptotic convergence to a Bayes-Optimal predictor.

This is due to the fact that $E_{y_1, \dots, y_K} \left[\frac{K}{K-1} \overline{Var}(y_1, \dots, y_K) \right] = Var_{P(y|x)}[y|x]$, which according to Proposition 1 is equal to $\mathcal{A}(x)$.

Algorithm 3 DEUP with a fixed training set: Training procedure to obtain estimates of epistemic uncertainty

Data: \mathcal{D} the training dataset with pairs (x, y) with $x \in \mathcal{X}$, $y \in \mathbb{R}$; \mathcal{D}_{out} the out-of-sample dataset with pairs (x, y) , to train the uncertainty estimator

\mathcal{X} , the input/search space

$a : \mathcal{X} \mapsto \mathbb{R}$, trained estimator of aleatoric uncertainty (

$f : \mathcal{X} \mapsto \mathbb{R}$, main predictor, trained on \mathcal{D}

$u : \mathcal{X} \mapsto \mathbb{R}$, total uncertainty estimator (estimates error of f)

Training:

Initialize empty dataset of errors \mathcal{D}_u

Optional: Pre-fill \mathcal{D}_u using Algorithm 2 and fit u on \mathcal{D}_u

$x_{acq} \leftarrow \emptyset, y_{acq} \leftarrow \emptyset$

for every pair (x, y) in $\mathcal{D} \cup \mathcal{D}_{out}$ do

 | $\mathcal{D}_u \leftarrow \mathcal{D}_u \cup \{(x, (y - f(x))^2)\}$

end

Fit u on \mathcal{D}_u

Evaluation: For every input x , return $u(x) - a(x)$ as an estimator of epistemic uncertainty at x

F Sequential Model Optimization Experiments

We use BoTorch³ [5] as the base framework for our experiments.

For all our Sequential Optimization algorithms, we use Algorithm 1 to train DEUP uncertainty estimators. We found that the optional step of pre-filling the uncertainty estimator dataset \mathcal{D}_e was important given the low number of available training points. We used half the initial training set (randomly chosen) as in-sample examples (used to train the main predictor and an extra-feature generator) and the other half as out-of-sample examples to provide instances of high epistemic uncertainty to train an uncertainty predictor; we repeated the procedure by alternating the roles of the two halves of the dataset. We repeated the whole procedure twice using a new random split of the dataset, thus ending up with 4 training points in \mathcal{D}_e for every initial training point in \mathcal{D}_{init} .

The error predictor is trained with the log targets (i.e. log MSE between predicted and observed error). This helps since the scale of the errors varies over multiple orders of magnitude.

Computationally, the training time of DEUP-EI depends on various choices (e.g. the features used to train the epistemic uncertainty predictor, the dimension of the input, the learning algorithms, etc.). Additionally, the training time for the uncertainty predictor varies at each step of the optimization. In total, the sequential optimization experiments took about 1 CPU day.

F.1 One-dimensional function toy example

In Figure 6, we show the results of DEUP-EI, compared to GP-EI, MCDropout-EI and Ensembles-EI, in the task of optimizing a synthetic one-dimensional function. Because MCDropout and Ensembles are trained on in-sample data only, they are unable to generalize their uncertainty estimates, which makes them bad candidates for Sequential Model Optimization, because they are easily stuck in local minima, and require many iterations before the acquisition function gives more weight to the predicted uncertainties than the current maximum.

For Random acquisition, we sampled for different seeds 56 points, and used the (average across the seeds of the) maximum of the first 6 values as the first value in the plots (Figures 3 and 6). Note that because the function is specifically designed to have multiple local maxima, GP-EI also required more optimization steps, and actually performed worse than random acquisition

As a stationarizing input feature, we used the variance of a GP fit on the available data at every step. We found that the binary (in-sample/out-of-sample) feature and density estimates were redundant with the variance feature and didn't improve the performance as captured by the number of additional function calls. We used a GP for the DEUP uncertainty estimator. Using a neural net provided similar results, but was computationally more expensive in this 1-D case with few datapoints. We used a

³<https://botorch.org/>

3-hidden layer neural network, with 128 neurons per layer and a ReLU activation function, with Adam [33] and a learning rate of 10^{-3} (and default values for the other hyperparameters) to train the main predictor for DEUP-EI (in order to fit the available data). The same network architecture and learning rate were used for the Dropout and Ensemble baselines. We used 3 networks for the Ensemble baseline, and a dropout probability of 0.3 for the Dropout baseline, with 100 test-time forward passes to compute uncertainty estimates.

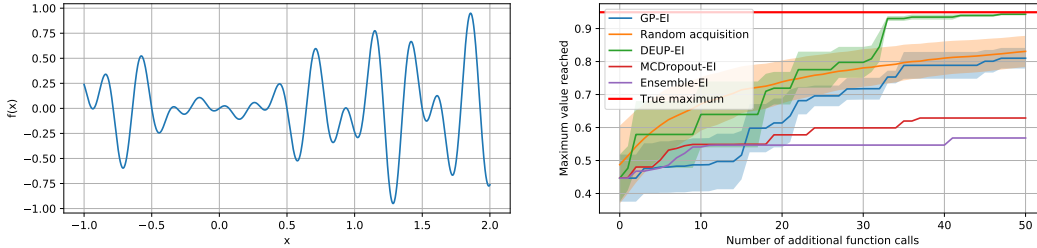


Figure 6: *Left.* Synthetic function to optimize. *Right.* Maximum value reached by the different methods on the synthetic function. The shaded areas represent the standard error across 5 different runs, with different initial sets of 6 pairs. For clarity, the shaded areas are omitted for the two worst performing methods. In each run, all the methods start with the same initial set of 6 points. GP-EI tends to get stuck in local optima and requires more than 50 steps, on average, to reach the global maximum.

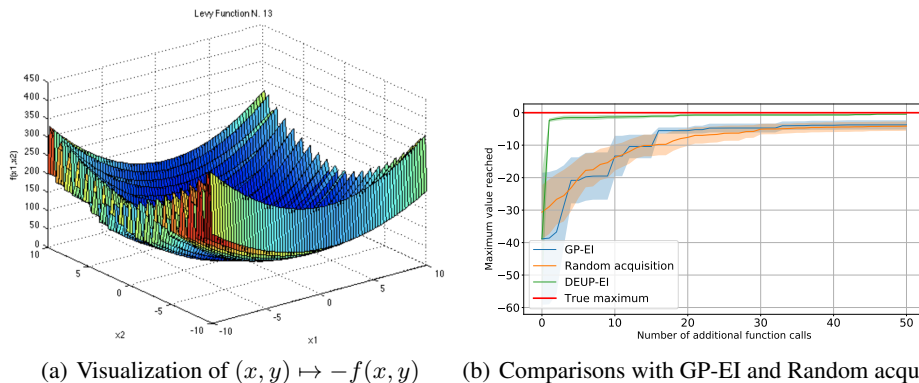
F.2 Two-dimensional function

To showcase DEUP’s usefulness for Sequential Model Optimization in with a number of dimensions greater than 1, we consider the optimization of the Levi N.13 function, a known benchmark for optimization. The function f takes a point (x, y) in 2D space and returns:

$$f(x, y) = -(\sin^2(3\pi x) + (x - 1)^2(1 + \sin^2(3\pi y)) + (y - 1)^2(1 + \sin^2(2\pi y)))$$

We use the box $[-10, 10]^2$ as the optimization domain. In this domain, the maximum of the function is 0, and it is reached at $(1, 1)$. The function has multiple local maxima, as shown in Figure 7(a)⁴.

Similar to the previous one-dimensional function, MCDropout and Ensemble provided bad performances and are omitted from the plot in 7(b). We used the same setting and hyperparameters for DEUP as for the previous function. DEUP-EI is again the only method that reaches the global maximum consistently in under 56 function evaluations.



(a) Visualization of $(x, y) \mapsto -f(x, y)$ (b) Comparisons with GP-EI and Random acquisition

Figure 7: Sequential Model Optimization on the Levi N.13 function

⁴Plot of the function copied from <https://www.sfu.ca/ssurjano/levy13.html>

F.3 Additional details for the Ackley function experiment, for synthetic data in higher dimensions

The Ackley function of dimension d is defined as:

$$\text{Ackley}_d : \mathcal{B} \rightarrow \mathbb{R}$$
$$x \mapsto A \exp \left(-B \sqrt{\frac{1}{d} \sum_{i=1}^d x_i^2} \right) + \exp \left(\frac{1}{d} \sum_{i=1}^d \cos(cx_i) \right) - A - \exp(1)$$

where \mathcal{B} is a hyperrectangle of \mathbb{R}^d . $(0, \dots, 0)$ is the only global optimizer of Ackley_d , at which the function is equal to 0. We use BoTorch’s default values for A, B, c , which are 20, 0.2, 2π respectively.

In our experiments, we used $\mathcal{B} = [-10, 15]^d$ for all dimensions d .

For the TurBO baseline, we use BoTorch’s default implementation, with Expected Improvement as an acquisition function, and a batch size of 1 (i.e. acquiring one point per step).

For fair comparisons, for DEUP, we use a Gaussian Process as the main model, and use its variance as the only input of the epistemic uncertainty predictor. This means that we calibrate the GP variance to match the out-of-sample squared error, using another GP to perform the regression. TurBO-DEUP is a combination of both, in which we perform the variance calibration task for the local GP models of TurBO. The uncertainty predictor, i.e. the GP regressor, is trained with log targets, as in Appendix F.1, but also with log variances as inputs.

Note that only the stationarizing feature is used as input for the uncertainty predictor. When we used the input x as well, we found that the GP error predictor overfits on the x part of the input (x, v) , and it was detrimental to the final performances. For all experiments, we used 20 initial points.

G Reinforcement Learning Experiments

For RL experiments, we used *bsuite* [60], a collection of carefully designed RL environments. *bsuite* also comes with a list of metrics which aim to evaluate RL agents from different aspects. We compare the agents based on the *basic* metric and average regret as they capture both sample complexity and final performance. The default DQN agent is used as the base of our experiments with a 3 layer fully-connected (FC) neural network as its Q-network. For the Bootstrapped DQN baseline, we used the default implementation provided by *bsuite*. To implement DQN + MC-Dropout, following the implementation from [22], two dropout layers with dropout probability of 0.1 are used before the second and the third FC layers. In order to take an action, the agent performs a single stochastic forward pass through the Q-network, which is equivalent to taking a sample from the posterior over the Q-values, as done in Thompson sampling, an alternative to ϵ -greedy exploration.

As a density estimator, we used a Kernel Density Estimator (KDE) with a Gaussian kernel and bandwidth of 1 to map states to densities. This KDE is fit after each 10000 steps (actions) with a batch of samples from the replay buffer (which is of size 10000). The uncertainty estimator network (E-network) has the same number of layers as the Q-network, with an additional Softplus layer at the end. All other hyperparameters are the same as the default implementation by [60]. One complete training run for the DEUP-DQN with 5 seeds experiments takes about 0.04-0.05 GPU days on a V100 GPU. In total RL experiments took about 0.15 GPU days on a Nvidia V100 GPU.

Algorithm 4 DEUP-DQN

Initialize replay buffer \mathcal{D} with capacity \mathcal{N}
 $Q_\theta(s, a)$: state-action value predictor
 $E_\phi(\log d)$: uncertainty estimator network, which takes the log-density of the states as the input
 $d(s)$: Kernel density estimator (KDE)
 K : KDE fitting frequency
 W : Number of warm-up episodes
for $episode=1$ to M **do**
 set s_0 as the initial state
 for $t=1$ to $max-steps-per-episode$ **do**
 with probability ϵ : take a random action, **otherwise**:
 if $episode \leq W$: $a = \max_a Q_\theta(s_t, a)$, **else**: $a = \max_a [Q_\theta(s_t, a) + \kappa \times E_\phi(\log d(s_t))(a)]$
 store (s_t, a_t, r_t, s_{t+1}) in \mathcal{D}
 Sample random minibatch B of transitions (s_j, a_j, r_j, s_{j+1}) from \mathcal{D}
 if s_j is a final state: $y_j = r_j$, **else**: $y_j = r_j + \gamma \max_a Q(s_t, a)$
 Update Q-network:
 $\theta \leftarrow \theta + \alpha_Q \cdot \nabla_\theta \mathbb{E}_{(s,a) \sim B} [(y_j - Q_\theta(s, a))^2]$
 Update E-network:
 $\phi \leftarrow \phi + \alpha_E \cdot \nabla_\phi \mathbb{E}_{(s,a) \sim B} \left[\left[(y_j - Q_\theta(s, a))^2 - E_\phi(\log d(s_t))(a) \right]^2 \right]$
 if $\text{mod}(\text{total-steps}, K) = 0$: fit the KDE d on the states of \mathcal{D}
 end
end

H Rejecting Difficult Examples

We adapt the standard OOD rejection task [76, 43] to measure the Spearman Rank Correlation of the predicted uncertainty with the true generalization error, in addition to the OOD Detection AUROC. We use MC-Dropout [22], Deep Ensemble [40], DUE[75] and DUQ [76] as the baselines⁵. We use these baselines as representatives for the major approaches for uncertainty estimation in recent literature. For all the methods, including DEUP we consider two architectures for the main predictor, ResNet-18 and ResNet-50 [24] (Table 2) to study the effect of model capacity. Note that for the ResNet50 DEUP model we continue using the ResNet-18 based DUE as variance source.

Table 2: Spearman Rank Correlation between predicted uncertainty and the true generalization error on OOD data (SVHN) with ResNet-50 models (3 seeds) trained on CIFAR-10.

Model	ResNet-50
MC-Dropout	0.312 ± 0.003
Deep Ensemble	0.401 ± 0.004
DUQ	0.399 ± 0.003
DEUP (D+V)	0.465 ± 0.002

Training The baselines were trained with the CIFAR-10 training set with 10% set aside as a validation set for hyperparameter tuning. The hyperparameters are presented in Table 3 and Table 4. The hyperparameters not specified are set to the default values. For DEUP, we consider the log-density, model-variance estimate and the seen-unseen bit as the features for the error predictor. The density estimator we use is Masked-Autoregressive Flows [62] and the variance estimator used is DUE [75]. Note that as indicated earlier x , the input image, is not used as a feature for the error predictor. We present those ablations in the next sub-section. For training DEUP, the CIFAR-10 training set is divided into 5 folds, with each fold containing 8 unique classes. For each fold, we

⁵MC-Dropout and Deep Ensemble baselines are based on <https://github.com/google/uncertainty-baselines>, DUQ based on <https://github.com/y0ast/deterministic-uncertainty-quantification> and DUE based on <https://github.com/y0ast/DUE>

train an instance of the main predictor, density estimator and model variance estimator on only the corresponding 8 classes. The remaining 2 classes act as the out-of-distribution examples for training the error predictor. Using these folds we construct a dataset for training the error predictor, a simple feed forward network. The error predictor is trained with the log targets (i.e. log MSE between predicted and observed error). This helps since the scale of the errors varies over multiple orders of magnitude. We then train the main predictor, density estimator and the variance estimator on the entire CIFAR-10 dataset, for evaluation. The hyperparameters are presented in Table 4. For all models, we train the main predictor for 75 and 125 epochs for ResNet-18 and ResNet-50 respectively. We use SGD with Momentum (set to 0.9), with a multi-step learning schedule with a decay of 0.2 at epochs [25, 50] and [45, 90] for ResNet-18 and ResNet-50 respectively. One complete training run for DEUP takes about 1.5-2 GPU days on a V100 GPU. In total these set of experiments took about 31 GPU days on a Nvidia V100 GPU.

Table 3: **Left:** Hyperparameters for training Deep Ensemble [40]. **Right:** Hyperparameters for training MC-Dropout [22].

Parameters	Model		Parameters	Model	
	ResNet-18	ResNet-50		ResNet-18	ResNet-50
Number of members	5	5	Number of samples	50	50
Learning Rate	0.05	0.01	Dropout Rate	0.15	0.1
			L2 Regularization Coefficient	6e-5	8e-4
			Learning Rate	0.05	0.01

Table 4: **Left:** Hyperparameters for training DUQ [76]. **Right:** Hyperparameters for training DUE [75].

Parameters	Model		Parameters	Model
	ResNet-18	ResNet-50		ResNet-18
Gradient Penalty	0.5	0.65	Inducing Points	50
Centroid Size	512	512	Kernel	RBF
Length scale	0.1	0.2	Lipschitz Coefficient	2
Learning Rate	0.05	0.025	BatchNorm Momentum	0.99
			Learning Rate	0.05
			Weight Decay	0.0005

Ablations We also perform some ablation experiments to study the effect of each feature for the error predictor. The Spearman rank correlation coefficient between the generalization error and the variance feature, V , from DUE [75] alone is 37.84 ± 0.04 , and the log-density, D , from MAF [62] alone is 30.52 ± 0.03 . With only the image (x) the SRCC is 36.58 ± 0.16

Table 6 presents the results for these experiments. We observe that combining all the features performs the best. Also note that using the log-density and variance as features to the error predictor we observe better performance than using them directly, indicating that the error predictor perhaps captures a better target for the epistemic uncertainty. The boolean feature (B) indicating seen examples, discussed in Section 2.2, also leads to noticeable improvements.

H.1 Predicting Uncertainty under Distribution Shift

We also consider the task of uncertainty estimation in the setting of shifted distributions [61, 25]. We evaluate the uncertainty predictions of models trained with CIFAR-10, on CIFAR-10-C [25] which

Table 5: Hyperparameters for training DEUP.

Parameters	Model	
	ResNet-18	ResNet-50
Uncertainty Predictor Architecture	[1024] x 5	[1024] x 5
Uncertainty Predictor Epochs	100	100
Uncertainty Predictor LR	0.01	0.01
Main Predictor Learning Rate	0.05	0.01

Table 6: Spearman Rank Correlation between predicted uncertainty and the true generalization error on OOD data (SVHN) with variants of DEUP with different features as input for the uncertainty predictor. D indicates the log-density from MAF [62], V indicates variance from DUQ [76] and B indicates a bit indicating if the data is seen.

Features	Model	
	ResNet-18	ResNet-50
$D+V+B$	0.426 ± 0.009	0.465 ± 0.002
$D+V$	0.419 ± 0.003	0.447 ± 0.003
$V+B$	0.401 ± 0.004	0.419 ± 0.004
$D+B$	0.403 ± 0.003	0.421 ± 0.002

consists of images from CIFAR-10 distorted using 16 corruptions like gaussian blur, impulse noise, among others. Figure 8 shows that even in the shifted distribution setting, the uncertainty estimates of DEUP correlate much better with the error made by the predictor, compared to the baselines.

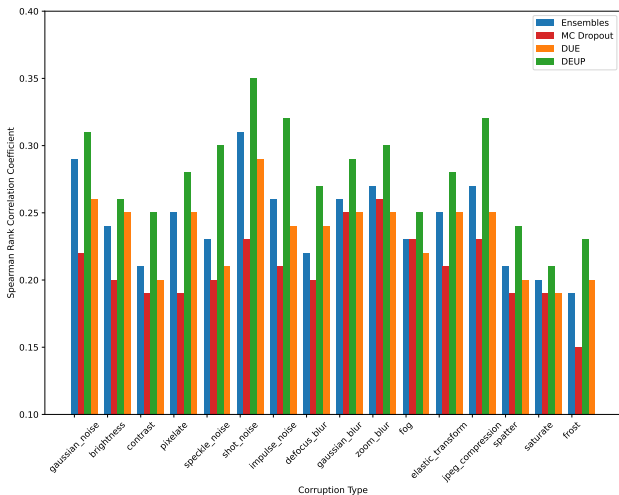


Figure 8: Spearman Rank Correlation Coefficient between the predicted uncertainty and true error for models trained with CIFAR-10, and evaluated on CIFAR-10-C. DEUP outperforms the baselines on all types of corruptions.

I Drug Combination Experiments

To validate DEUP’s uncertainty estimates in a real-world setting, we measured its performance on a regression task predicting the synergy of drug combinations. While much effort in drug discovery is spent on finding novel small molecules, a potentially cheaper method is identifying combinations of pre-existing drugs which are synergistic (i.e., work well together). Indeed, drug combinations are the current standard-of-care for a number of diseases including HIV, tuberculosis, and some cancers [15, 58, 53].

However, due to the combinatorial nature of drug combinations, identifying pairs exhibiting synergism is challenging. Compounding this problem is the high monetary cost of running experiments on promising drug combinations, as well as the length of time the experiments take to complete. Uncertainty models could be used by practitioners downstream to help accelerate drug combination treatment discoveries and reduce involved development costs.

To test DEUP’s performance on this task we used the DrugComb and LINCS L1000 datasets [82, 69]. DrugComb is a dataset consisting of pairwise combinations of anti-cancer compounds tested on various cancer cell lines. For each combination, the dataset provides access to several synergy scores,

each indicating whether the two drugs have a synergistic or antagonistic effect on cancerous cell death. LINCS L1000 contains differential gene expression profiles for various cell lines and drugs. Differential gene expressions measure the difference in the amount of mRNA related to a set of influential genes before and after the application of a drug. Because of this, gene expressions are a powerful indicator of the effect of a single drug at the cellular level.

In our experiments, each drug is represented by its Morgan fingerprint [54]⁶ (with 1,024 bits and a radius of 3) as well as two differential gene expression profiles (each of dimension 978) from two cell lines (PC-3 and MCF-7). In order to use gene expression features for every drug, we only used drug pairs in DrugComb where both drugs had differential gene expression data for cell lines PC-3 and MCF-7.

We first compared the quality of DEUP’s uncertainty estimations to other uncertainty estimation methods on the task of predicting the combination sensitivity score [49] for drug pairs tested on the cell line PC-3 (1,385 examples). We evaluated the uncertainty methods using a train, validation, test split of 40%, 30%, and 30%, respectively. The underlying model used by each uncertainty estimation method consisted of a *single drug* fully connected neural network (2 layers with 2048 hidden units and output of dimension 1024) and a *combined drug* fully connected neural network (2 layers, with 128 hidden units). The embeddings of an input drug pair’s drugs produced by the *single drug* network are summed and passed to the *combined drug* network, which then predicts final synergy. By summing the embeddings produced by the *single drug* network, we ensure that the model is invariant to permutations in order of the two drugs in the pair. The models were trained with Adam [33], using a learning rate of 1e-4 and weight decay of 1e-5. For MC-Dropout we used a dropout probability of 0.1 on the two layers of the *combined drug* network and 3 test-time forward passes to compute uncertainty estimates. The ensemble used 3 constituent models for its uncertainty estimates. Both Ensemble and MC-Dropout models were trained with the *MSE* loss.

We also compared against DUE [75] which combines a neural network feature extractor with an approximate Gaussian process. Spectral normalization was added to all the layers of the *combined drug* network and of the *single drug* network. Let d_{emb} denote the dimension of the output of the *combined drug* network, which is also the input dimension of the approximate Gaussian process. We conducted a grid-search over different values of d_{emb} (from 2 to 100), the number of *inducing points* (from 3 to 200), the learning rate, and the kernel used by the Gaussian process. The highest correlation of uncertainty estimates with residuals was attained with $d_{\text{emb}} = 10$, 100 *inducing points*, a learning rate of 1e-2, and the *Matern12* kernel.

⁶The Morgan fingerprint represents a molecule by associating with it a boolean vector specifying its chemical structure. Morgan fingerprints have been used as a signal of various molecular characteristics to great success [6, 84].

Algorithm 5 DEUP for Drug Combinations

Data: \mathcal{D} dataset of pairwise drug combinations, along with synergy scores $((d_1, d_2), y)$

Initialization:

Split training set into two halves, *in-sample* \mathcal{D}_{in} and *out-of-sample* \mathcal{D}_{out}

$f_\mu(d_1, d_2)$: $\hat{\mu}$ predictor which takes a pair of drugs as input

$f_\sigma^{in}(d_1, d_2)$: In-sample $\hat{\sigma}_{in}$ error predictor

$f_\sigma^{out}(d_1, d_2)$: Out-of-sample $\hat{\sigma}_{out}$ error predictor

Training:

while training not finished do

In-sample update

 Get an *in-sample* batch $(d_{1,in}, d_{2,in}, y_{in}) \sim \mathcal{D}_{in}$

 Predict $\hat{\mu} = f_\mu(d_{1,in}, d_{2,in})$ and *in-sample* error $\hat{\sigma}_{in} = f_\sigma^{in}(d_{1,in}, d_{2,in})$

 Compute *NLL*: $\frac{\log(\hat{\sigma}_{in}^2)}{2} + \frac{(\hat{\mu} - y_{in})^2}{2\hat{\sigma}_{in}^2}$

 Backpropagate through f_μ and f_σ^{in} and update.

Out-of-sample update

 Get an *out-of-sample* batch $(d_{1,out}, d_{2,out}, y_{out}) \sim \mathcal{D}_{out}$

 Estimate $\hat{\mu} = f_\mu(d_{1,out}, d_{2,out})$ and *out-of-sample* error $\hat{\sigma}_{out} = f_\sigma^{out}(d_{1,out}, d_{2,out})$

 Compute *NLL*: $\frac{\log(\hat{\sigma}_{out}^2)}{2} + \frac{(\hat{\mu} - y_{out})^2}{2\hat{\sigma}_{out}^2}$

 Backpropagate through f_σ^{out} and update.

end

The DEUP model we used outputs two heads $\begin{bmatrix} \hat{\mu} \\ \hat{\sigma} \end{bmatrix}$ and is trained with the *NLL* $\frac{\log(\hat{\sigma}^2)}{2} + \frac{(\hat{\mu} - y)^2}{2\hat{\sigma}^2}$ in a similar fashion as in [40]. To obtain a predictor of the out-of-sample error, we altered our optimization procedure so that the μ and σ heads were not backpropagated through at all times. Specifically, we first split the training set into two halves, terming the former the in-sample set \mathcal{D}_{in} and the latter the out-of-sample set \mathcal{D}_{out} . We denote as f_σ^{in} the in-sample error predictor and f_σ^{out} the out-of-sample error predictor. f_σ^{out} is used to estimate total uncertainty. Note that in this setting, f_σ^{out} predicts the square root of the epistemic uncertainty ($\hat{\sigma}_{out}$) rather than the epistemic uncertainty itself ($\hat{\sigma}_{out}^2$).

In our experiments, an extra bit is added as input to the model in order to indicate whether a given batch is from \mathcal{D}_{in} or \mathcal{D}_{out} . Through this, the same model is used to estimate f_σ^{in} and f_σ^{out} with the model estimating f_σ^{in} when the bit indicates an example is drawn from \mathcal{D}_{in} and f_σ^{out} otherwise. When the batch is drawn from \mathcal{D}_{in} , both heads are trained using *NLL* using a single forward pass. However, when the data is drawn from \mathcal{D}_{out} only the $\hat{\sigma}$ head is trained. To do this, we must still predict $\hat{\mu}$ in order to compute the *NLL*. But the $\hat{\mu}$ predictor f_μ must be agnostic to the difference between \mathcal{D}_{in} and \mathcal{D}_{out} . To solve this, we perform two separate forward passes. The first pass computes $\hat{\mu}$ and sets the indicator bit to 0 so f_μ has no notion of \mathcal{D}_{out} , while the second pass computes $\hat{\sigma}$, setting the bit to 1 to indicate the true source of the batch. Finally, we backpropagate through the $\hat{\sigma}$ head only. The training procedure is described in Algorithm 5

We report several measures for the quality of uncertainty predictions on a separate test set in Table 7.

Model	Corr. w. res.	U. Bound	Ratio	Log Likelihood	Coverage Probability	CI width
MC-Dropout	0.14 ± 0.07	0.56 ± 0.05	0.25 ± 0.12	-20.1 ± 6.8	11.4 ± 0.2	3.1 ± 0.1
Deep Ensemble	0.30 ± 0.09	0.59 ± 0.04	0.50 ± 0.13	-14.3 ± 4.7	10.8 ± 1.4	3.4 ± 0.6
DUE	0.12 ± 0.12	0.15 ± 0.03	0.80 ± 0.79	-13.0 ± 0.52	15.2 ± 1.0	3.5 ± 0.1
DEUP	0.47 ± 0.03	0.63 ± 0.05	0.75 ± 0.07	-3.5 ± 0.25	36.1 ± 2.5	13.1 ± 0.9

Table 7: Drug combinations: quality of uncertainty estimates from different methods. *Corr. w. res.* shows correlation between model residuals and predicted uncertainties $\hat{\sigma}$. A best-case *Upper Bound* on *Corr. w. res.* is obtained from the correlation between $\hat{\sigma}$ and true samples from $\mathcal{N}(0, \hat{\sigma})$. *Ratio* is the ratio between col. 1 and 2 (larger is better). *Log-likelihood*: average over 3 seeds of per sample predictive log-likelihood. *Coverage Probability*: Percentage of test samples which are covered by the 68% confidence interval. *CI width*: width of the 86% confidence interval.

For each model, we report the per sample predictive log-likelihood, coverage probability and confidence interval width, averaged over 3 seeds.

We also computed the correlation between the residuals of the model $|\hat{\mu}(x_i) - y_i|$ and the predicted uncertainties $\hat{\sigma}(x_i)$. We noted that the different uncertainty estimation methods lead to different distributions $p(\hat{\sigma}(x))$. For example, predicted uncertainties obtained with DUE always have a similar magnitude. By contrast, DEUP yields a wide range of different predicted uncertainties.

These differences between the distributions $p(\hat{\sigma}(x))$ obtained with the different methods may have an impact on the correlation metric, possibly biasing the comparison of the different methods. In order to account for differences in the distribution $p(\hat{\sigma}(x))$ across methods, we report another metric which is the ratio between the observed correlation $Corr(|\hat{\mu}(x) - y|, \hat{\sigma}(x))$ and the maximum achievable correlation given a specific distribution $p(\hat{\sigma}(x))$.

This maximum achievable correlation (referred to as the *upper bound*) is not *per se* a comparison metric, and is estimated (given a specific $p(\hat{\sigma}(x))$) as follows: we assume that, for each example (x_i, y_i) , the predictive distribution of the model $\mathcal{N}(\hat{\mu}(x_i), \hat{\sigma}(x_i))$ corresponds exactly to the distribution of the target, i.e. $y_i \sim \mathcal{N}(\hat{\mu}(x_i), \hat{\sigma}(x_i))$. Under this assumption, the residual of the mean predictor follows a distribution $\mathcal{N}(0, \hat{\sigma}(x_i))$. We can then estimate the upper bound by computing the correlation between the predicted uncertainties $\hat{\sigma}(x_i)$ and samples from the corresponding Gaussians $\mathcal{N}(0, \hat{\sigma}(x_i))$. 5 samples were drawn from each Gaussian for our evaluation. This upper bound is reported in the Table.

Finally, we reported our comparison metric: the ratio between the correlation $Corr(|\hat{\mu}(x) - y|, \hat{\sigma}(x))$ and the upper bound. The higher the ratio is, the closer the observed correlation is to the estimated upper bound and the better the method is doing.

It is interesting to note that the upper bound is much lower for DUE compared to other methods, as its predicted uncertainties lie within a short range of values.

Predicted $\hat{\mu}$ and uncertainty estimates can be visualized in Figure 9 for different models. MC-dropout, Ensemble and DUE consistently underestimate uncertainty, while the out-of-sample uncertainties predicted by DEUP are much more consistent with the order of magnitude of the residuals. Moreover, we observed that DUE predicted very similar uncertainties for all samples, resulting in a lower upper-bound for the correlation between residuals and predicted uncertainties compared to other methods. We observed a similar pattern when experimenting with the other kernels available in the DUE package, including the standard Gaussian kernel.

Finally, we note that in the context of drug combination experiments, aleatoric uncertainty could be estimated by having access to replicates of a given experiment (*c.f.* Section E), allowing us to subtract the aleatoric part from the out-of-sample uncertainty, leaving us with the epistemic uncertainty only.

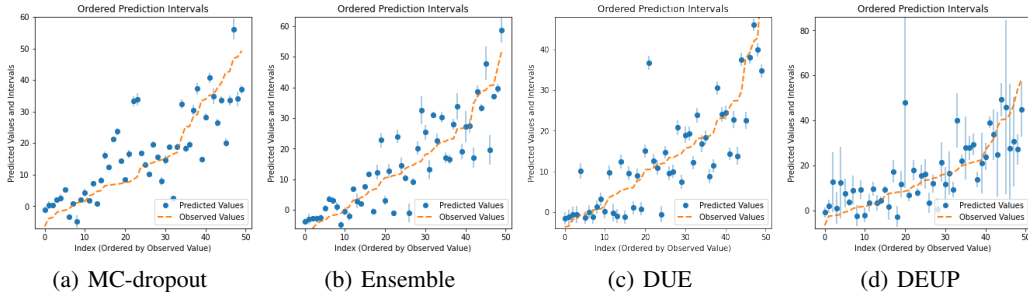


Figure 9: Predicted mean and uncertainty for different models on a separate test set. 50 examples from the test set are ordered by increasing value of true synergy score (orange). Model predictions and uncertainties are visualized in blue. MC-Dropout, Ensemble and DUE consistently underestimate the uncertainty while DEUP seems to capture the right order of magnitude. Figures made using The Uncertainty Toolbox [14].

One complete training run for the drug combination experiments takes about 0.01 GPU days on a V100 GPU. In total these set of experiments took about 0.2 GPU days on a Nvidia V100 GPU.